The Astrophysical Journal, 827:132 (29pp), 2016 August 20 doi:10.3847/0004-637X/827/2/132

COMPLEX HYDROCARBON CHEMISTRY IN INTERSTELLAR AND SOLAR SYSTEM ICES REVEALED: A COMBINED INFRARED SPECTROSCOPY AND REFLECTRON TIME-OF-FLIGHT MASS SPECTROMETRY ANALYSIS OF ETHANE (C_2H_6) AND D6-ETHANE (C_2D_6) ICES EXPOSED TO IONIZING RADIATION

Matthew J. Abplanalp[1,2] and Ralf I. Kaiser[1,2]
[1] W. M. Keck Research Laboratory in Astrochemistry, University of Hawaii at Manoa, Honolulu, HI 96822, USA; ralfk@hawaii.edu
[2] Department of Chemistry, University of Hawaii at Manoa, Honolulu, HI 96822, USA
Received 2016 April 11; revised 2016 June 13; accepted 2016 June 14; published 2016 August 16

ABSTRACT

The irradiation of pure ethane (C_2H_6/C_2D_6) ices at 5.5 K, under ultrahigh vacuum conditions was conducted to investigate the formation of complex hydrocarbons via interaction with energetic electrons simulating the secondary electrons produced in the track of galactic cosmic rays. The chemical modifications of the ices were monitored in situ using Fourier transform infrared spectroscopy (FTIR) and during temperature-programmed desorption via mass spectrometry exploiting a quadrupole mass spectrometer with electron impact ionization (EI-QMS) as well as a reflectron time-of-flight mass spectrometer coupled to a photoionization source (PI-ReTOF-MS). FTIR confirmed previous ethane studies by detecting six molecules: methane (CH_4), acetylene (C_2H_2), ethylene (C_2H_4), the ethyl radical (C_2H_5), 1-butene (C_4H_8), and *n*-butane (C_4H_{10}). However, the TPD phase, along with EI-QMS, and most importantly, PI-ReTOF-MS, revealed the formation of at least 23 hydrocarbons, many for the first time in ethane ice, which can be arranged in four groups with an increasing carbon-to-hydrogen ratio: C_nH_{2n+2} ($n = 3$, 4, 6, 8, 10), C_nH_{2n} ($n = 3$–10), C_nH_{2n-2} ($n = 3$–10), and C_nH_{2n-4} ($n = 4$–6). The processing of simple ethane ices is relevant to the hydrocarbon chemistry in the interstellar medium, as ethane has been shown to be a major product of methane, as well as in the outer solar system. These data reveal that the processing of ethane ices can synthesize several key hydrocarbons such as C_3H_4 and C_4H_6 isomers, which have been found to synthesize polycyclic aromatic hydrocarbons like indene (C_9H_8) and naphthalene ($C_{10}H_8$) in the ISM and in hydrocarbon-rich atmospheres of planets and their moons such as Titan.

Key words: astrochemistry – cosmic rays – infrared: general – ISM: molecules – methods: laboratory: solid state – radiation mechanisms: non-thermal

1. INTRODUCTION

The detection of ethane (C_2H_6) in the atmospheres of the planets Jupiter, Saturn, Uranus, and Neptune (Gillett & Forrest 1974; Ridgway 1974; Hammel et al. 2006) as well as in Titan, Pluto, Quaoar, Makemake (Nakamura et al. 2000; Niemann et al. 2005; Griffith et al. 2006; Dalle Ore et al. 2009; Holler et al. 2014; Brown et al. 2015), and comets including C/1996 B2 Hyakutake, 153P/Ikeya-Zhang, C/2001 A2, and C/1999 H1 (DiSanti & Mumma 2008), shows that ethane is a common molecule that deserves the attention of the astrochemistry community. According to Mumma et al. (1996), ethane detected in comet C/1996 B2 Hyakutake is likely of interstellar origin based upon its relative abundance to water and can be traced back to the energetic processing of methane ice (Boogert et al. 2015) in interstellar clouds, as shown in laboratory experiments simulating the irradiation of pure methane ice (Gerakines et al. 1996; Kaiser & Roessler 1998; Bennett et al. 2006; Jones & Kaiser 2013), and in mixtures of methane with water (Moore & Hudson 1998) by ionizing radiation. Titan has been a main focus for the study of ethane (Kim et al. 2010). This moon of Saturn has an atmosphere consisting primarily of nitrogen (98.4%) and methane (1.4%) (Niemann et al. 2005). However, the Cassini mission was able to detect clouds of ethane aerosol particles (Griffith et al. 2006), and the Huygens spacecraft's landing site provided evidence of ethane as well (Niemann et al. 2005). The origin of ethane is most likely based on its formation via methane photodissociation followed by transport to the surface of Titan (Lavvas et al. 2008). Hunten et al. suggested that ethane is most likely sequestered in organic hazes, which then leads to cloud formation followed by sedimentation and transfer to the surface (Hunten 2006). Titan has been determined to have mixed methane and ethane lakes (Mousis et al. 2016).

However, a literature review suggests that very few laboratory experiments investigating the effects of ionizing radiation on ethane ices are available. The ultraviolet (UV) photolysis of solid ethane has been studied for its decomposition pathways and researchers have detected hydrocarbons as large as butane isomers (C_4H_{10}) (Scheer et al. 1962; Jackson et al. 1966). Dartois et al. (2005) describe more recent UV photolysis experiments of ethane resulting in the formation of "complex residues." Also, ion implantation experiments using 200 keV protons processed ethane ices, which yielded ethylene (C_2H_4) and acetylene (C_2H_2) as monitored via Raman spectroscopy (Compagnini et al. 2009). The processing of amorphous ethane ice with 0.8 MeV protons formed methane (CH_4), acetylene (C_2H_2), ethylene (C_2H_4), *n*-butane (C_4H_{10}), and hydrocarbons belonging to the generic formula C_3H_x ($x =$ 4, 6, 8) (Hudson et al. 2009). Ion implantation experiments using 30 keV He^+ were also conducted, resulting in the quantification of ethane destruction rates as well as the detection of methane, acetylene, and ethylene (Strazzulla et al. 2002). Ethane ices were also processed with 15 keV N^+ ions, which rose to the infrared detection of the nitrile functional group (-C ≡ N) in hydrogen cyanide (HCN) (Strazzulla et al. 2002). Finally, the study of solid ethane exposed to 5 keV electrons detected molecules as large as *n*-butane (Kim et al. 2010), where the energetic electrons simulate secondary electrons generated in the track of galactic cosmic rays (GCRs) (Charnley et al. 2001). Combined, these

aforementioned studies exploited a broad set of analytical techniques ranging from offline and ex situ mass spectrometry and gas chromatography to online and in situ infrared spectroscopy (FTIR) along with quadrupole mass spectrometry coupled with electron impact ionization (EI-QMS).

However, although ethane has been an important molecule in both laboratory and observational astrochemistry, to date, the radiation products have not been probed by more sensitive techniques either online or in situ. FTIR has been a primary tool used to monitor the effects of radiation on astrophysical ice analogs in the laboratory (Khare et al. 1989; Moore et al. 1996; Caro & Schutte 2003; Abplanalp et al. 2016). However, infrared spectroscopy is truly only useful when utilized to identify small (individual) molecules like carbon monoxide (CO), water (H_2O), carbon dioxide (CO_2), methane (CH_4), acetylene (C_2H_2), ethylene (C_2H_4), and ammonia (NH_3), based on the vibrations associated with a change in the permanent dipole moment of the molecule. The infrared spectra can also be exploited to identify functional groups such as those related to complex organic molecules (COMs) like carbonyl groups associated with aldehydes, ketones, and carboxylic acids (Socrates 2004). However, different molecules with the same functional groups will have similar vibrational frequencies differing by a few 10 cm^{-1} causing overlap in the infrared spectra observed; this limits the identification of individual molecules (Bennett et al. 2005b; Zhou et al. 2008). Due to these restrictions, FTIR aids in identifying small molecules and new functional groups of organics formed within the astrophysical ice analogs, but FTIR cannot always identify specific molecules of interest; therefore, the exclusive assignment of a single molecule to infrared bands in an unknown mixture of molecules is not advisable as many vibrational frequencies may overlap.

Further, a complementary analysis of the system in the gas phase is often conducted via temperature-programmed desorption (TPD) and probing the subliming molecules via mass spectrometry. Typically this is accomplished by operating an EI-QMS to identify newly formed molecules in the processed ices after their sublimation (Kaiser et al. 1995a, 1995b; Fraser et al. 2002; Ioppolo et al. 2011; Jiménez-Escobar & Caro 2011; Duvernay et al. 2014). The EI-QMS operating at 70–100 eV, where the ionization cross section of organic molecules is often at their maximum, readily ionizes molecules, but this ionization also causes substantial fragmentation (dissociative ionization) of the molecule; in the most unfavorable case, this results in a lack of the molecular parent ion altogether. Furthermore, the fragment ions of molecules, especially of structural isomers, often overlap making a confident assignment of structural isomers very difficult (Kaiser et al. 1997a, 2010; Kaiser & Roessler 1997; Bennett et al. 2005a; Bennett & Kaiser 2007). For example, a simple model ice mixture of carbon monoxide (CO) and methane (CH_4) would present a difficult detection of COMs such as acetaldehyde (CH_3CHO; $m/z = 44$) via EI-QMS because of contributing ion counts from both carbon dioxide (CO_2; $m/z = 44$) and propane (C_3H_8; $m/z = 44$), which are both principal products in processed carbon monoxide and methane ices (Kaiser et al. 2014). The situation is further complicated by the additional structural isomers, vinyl alcohol (H_2CCHOH) and ethylene oxide (c-C_2H_4O), all having the molecular formula of C_2H_4O ($m/z = 44$). Consequently, the traditional methods utilized to identify organic molecules in processed interstellar analog ices lack the capabilities needed to provide a detailed identification of the newly formed products.

Finally, a non-volatile residue—a complex mixture of often organic polymers—might be formed from the processing of carbon-bearing ices; this results in a substantial overlap of vibrational modes in the infrared spectrum (Kaiser & Roessler 1992; Modica et al. 2012; Callahan et al. 2013; Danger et al. 2013; de Marcellus et al. 2015). Although the infrared spectra of the residues can be deconvoluted, this leads to the identification of *functional groups* rather than specific molecules. Often these residues are analyzed offline via gas chromatography–mass spectrometry (GC–MS) (Meinert et al. 2012; Callahan et al. 2013; Abou Mrad et al. 2014; de Marcellus et al. 2015) which results in the exposure of the residue to chemical processing such as acid hydrolysis and derivatizing with volatile trimethylsilyl derivatives (-$Si(CH_3)_3$). It is likely that this processing leads to a modification and degradation of the residues (Fang et al. 2015).

Considering the limitations of these traditional analytical techniques (FTIR, QMS, GC–MS), it is clear that a different approach is required in laboratory astrophysics to understand the formation of organic molecules upon interaction of ionizing radiation with astrophysically relevant ices. The present study employs an alternative method of tunable photoionization coupled with reflectron time-of-flight mass spectrometry (PI-ReTOF-MS) to unravel the complex chemistry taking place in the irradiated ethane ices. The incorporation of fragment-free single photon soft photoionization utilizing tunable vacuum ultraviolet light (VUV) has previously demonstrated the feasibility of this approach (Jones & Kaiser 2013; Kaiser et al. 2014, 2015; Maity et al. 2014a, 2014b, 2015; Förstel et al. 2015; Maksyutenko et al. 2015; Turner et al. 2015, 2016; Abplanalp et al. 2016). The products released into the gas phase are photoionized and sampled via a reflectron time-of-flight mass spectrometer, which monitors the complete product spectrum simultaneously based on the mass-to-charge ratios of the neutral molecules after their ionization. By photoionizing the subliming molecules with a single VUV photon, the fragmentation of the molecular ion can be primarily avoided, which is the major problem that EI-QMS presents. Most importantly, we can resolve the existence of distinct structural isomers if each isomer has a distinct ionization energy. This is accomplished by tuning the photon energy, within a resolution of a few 0.01 eV, to selectively photoionize only one isomer. Therefore, molecules can be selectively photoionized according to their ionization energies, which is a versatile and powerful approach to identifying how the molecules formed that has been previously lacking in laboratory astrophysics experiments (Abplanalp et al. 2015; Forstel et al. 2016). Furthermore, the concurrent monitoring of both the ice (FTIR) and gas phases (PI-ReTOF-MS) allows for a cross correlation of the data to extract more accurately which infrared peaks belong to which molecule based on their appearance in the PI-ReTOF-MS data and decline in the FTIR spectra. In summary, PI-ReTOF-MS coupled with FTIR has been established as a powerful tool for detecting the complete inventory of molecules formed in laboratory astrophysics experiments (Jones & Kaiser 2013; Kaiser et al. 2014, 2015; Maity et al. 2014a, 2014b, 2015; Förstel et al. 2015; Maksyutenko et al. 2015; Turner et al. 2015, 2016; Abplanalp et al. 2016).

Table 1
Infrared Absorption Features Recorded Before and After the Irradiation of Ethane Ices (C_2H_6) at 5.5 K

Absorptions Before Irradiation (cm^{-1})	Absorptions After Irradiation (cm^{-1})	Assignment	Carrier	References
		(a)		
	4500	$\nu_2 + \nu_3$ (CH_4)	Combination	1
4400, 4357, 4321, 4272, 4251, 4177, 4161, 4126, 4100, 4070		$\nu_8 + \nu_{10}$, $\nu_2 + \nu_7$, $\nu_6 + \nu_{10}$, $\nu_1 + \nu_6$, $\nu_2 + \nu_5$, $\nu_7 + \nu_{12}$, $\nu_7 + \nu_{12}$, $\nu_8 + \nu_{11} + \nu_{12}$, $\nu_8 + \nu_{11} + \nu_{12}$, $\nu_5 + \nu_{12}$ (C_2H_6)	Combinations	2
	3314	$\nu_3 + \nu_4 + \nu_5$ (C_2H_2)	Combination	3
	3263	ν_3 (C_2H_2)	CH stretch	4
3257		$\nu_4 + \nu_7$ (C_2H_6)	Combination	5
	3105	ν_{10} (C_2H_5)	CH_2 asymmetric stretch	4, 6
	3092	ν_9 (C_2H_4)	CH_2 asymmetric stretch	7
	3062	ν_3 (CH_4)	Degenerate stretch	1
	3022	ν_3 (CH_4)	Degenerate stretch	1
	3008	ν_3 (CH_4)	Degenerate stretch	7
2974		ν_{10} (C_2H_6)	CH_3 degenerate stretch	7
2959		ν_1 (C_2H_6)	CH_3 symmetric stretch	8
2943		$\nu_8 + \nu_{11}$ (C_2H_6)	Combination	3, 7
2910		$\nu_8 + \nu_{11}$ (C_2H_6)	Combination	3, 7, 9, 10
2882		ν_5 (C_2H_6)	CH_3 symmetric stretch	7
	2860	ν_{29} (C_4H_{10})	CH_2symmetric stretch	4
2848		$\nu_2 + \nu_4 + \nu_{12}$ (C_2H_6)	Combination	5
2821		$\nu_6 + \nu_{11}$ (C_2H_6)	Combination	5
2735		$\nu_2 + \nu_6$ (C_2H_6)	Combination	4, 7
2645		$\nu_8 + \nu_{12}$ (C_2H_6)	Combination	5
2557		$\nu_6 + \nu_9$ (C_2H_6)	Combination	9
1464		ν_{11} (C_2H_6)	CH_3 degenerate deformation	7
1369		ν_6 (C_2H_6)	CH_3 symmetric deformation	7
	1300	ν_4 (CH_4)	Degenerate deformation	7
	964	ν_{35} (C_4H_{10})	CH_3 rock	4
	949	ν_7 (C_2H_4)	CH_2 wag	1
	912	ν_{26} (C_4H_8)	CH_2 wag	4
817		ν_{12} (C_2H_6)	CH_3 rock	1
	747	ν_5 (C_2H_2)	CCH bend	3, 4
	734	ν_{17} (C_4H_{10})	CH_2 rock	4
		(b)		
3381, 3270, 3220, 3195, 3161, 3118, 3043, 2945, 2809, 2683		$\nu_8 + \nu_{10}$, $\nu_2 + \nu_7$, $\nu_6 + \nu_{10}$, $\nu_1 + \nu_6$, $\nu_2 + \nu_5$, $\nu_7 + \nu_{12}$, $\nu_7 + \nu_{12}$, $\nu_8 + \nu_{11} + \nu_{12}$, $\nu_8 + \nu_{11} + \nu_{12}$, $\nu_5 + \nu_{12}$ (C_2D_6)	Overtones/Combinations	11–13
2436		$\nu_4 + \nu_{10}$ (C_2D_6)	Combination	7
	2423	ν_3 (C_2D_2)	CD stretch	7
	2250	ν_{10} (C_2D_5)/ν_{22} (C_4D_8)	CD_2 asymmetric stretch/CD asymmetric stretch	6, 14
2229		ν_{10} (C_2D_6)	CD_3 degenerate stretch	11, 13
2214		$\nu_2 + \nu_6$ (C_2D_6)	Combination	11–13
	2192	ν_{23} (C_4D_8)	CD_3 asymmetric stretch	14
	2183	ν_{11} (C_2D_4)	CD_2 symmetric stretch	15
2129		$\nu_6 + \nu_9$ (C_2D_6)	Combination	11–13
2077		ν_5 (C_2D_6)	CD_3 symmetric stretch	13
2029		$\nu_6 + \nu_9$ (C_2D_6)	Combination	11–13
2012		$\nu_8 + \nu_9$ (C_2D_6)	Combination	11–13
1893		$\nu_3 + \nu_6$ (C_2D_6)	Combination	11–13
1068		ν_{11} (C_2D_6)	CD_3 degenerate deformation	11, 13
1055		ν_6 (C_2D_6)	CH_3 symmetric deformation	11–13
	991	ν_4 (CD_4)	Degenerate deformation	6
	719	ν_7 (C_2D_4)/ν_{33} (C_4D_{10})	CD_2 wag	15, 16
593		ν_{12} (C_2D_6)	CD_3 rock	11, 13

References. (1) Bennett et al. (2006), (2) Herman (1998), (3) Yu-Jong et al. (2014), (4) Kim et al. (2010), (5) Hepp & Herman (1999), (6) Pacansky & Dupuis (1982), (7) Kaiser et al. (2014), (8) Bennett & Kaiser (2007), (9) Lattanzi et al. (2011), (10) Kim (2003), (11) Nyquist et al. (1957), (12) Kondo & Saëki (1973), (13) Wisnosky et al. (1983), (14) Levin et al. (1973), (15) Jacox (1962), (16) Murphy et al. (1991).

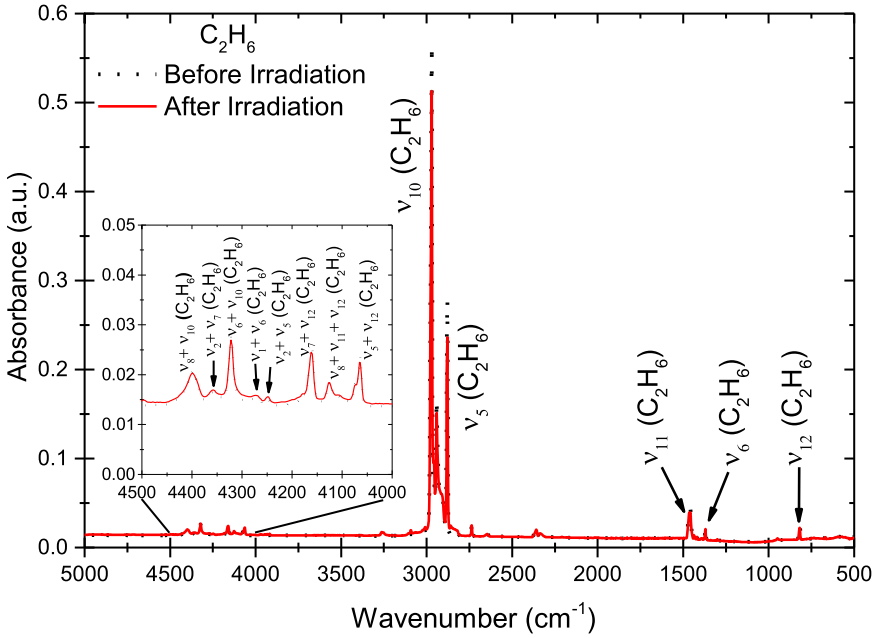

Figure 1. Infrared spectra from 5000 to 500 cm^{-1} for ethane (C_2H_6) ices before (black, dotted line) and after (red, solid line) the irradiation with a tenfold zoom of the overtones in the inset box along with assignments (Table 1(a)).

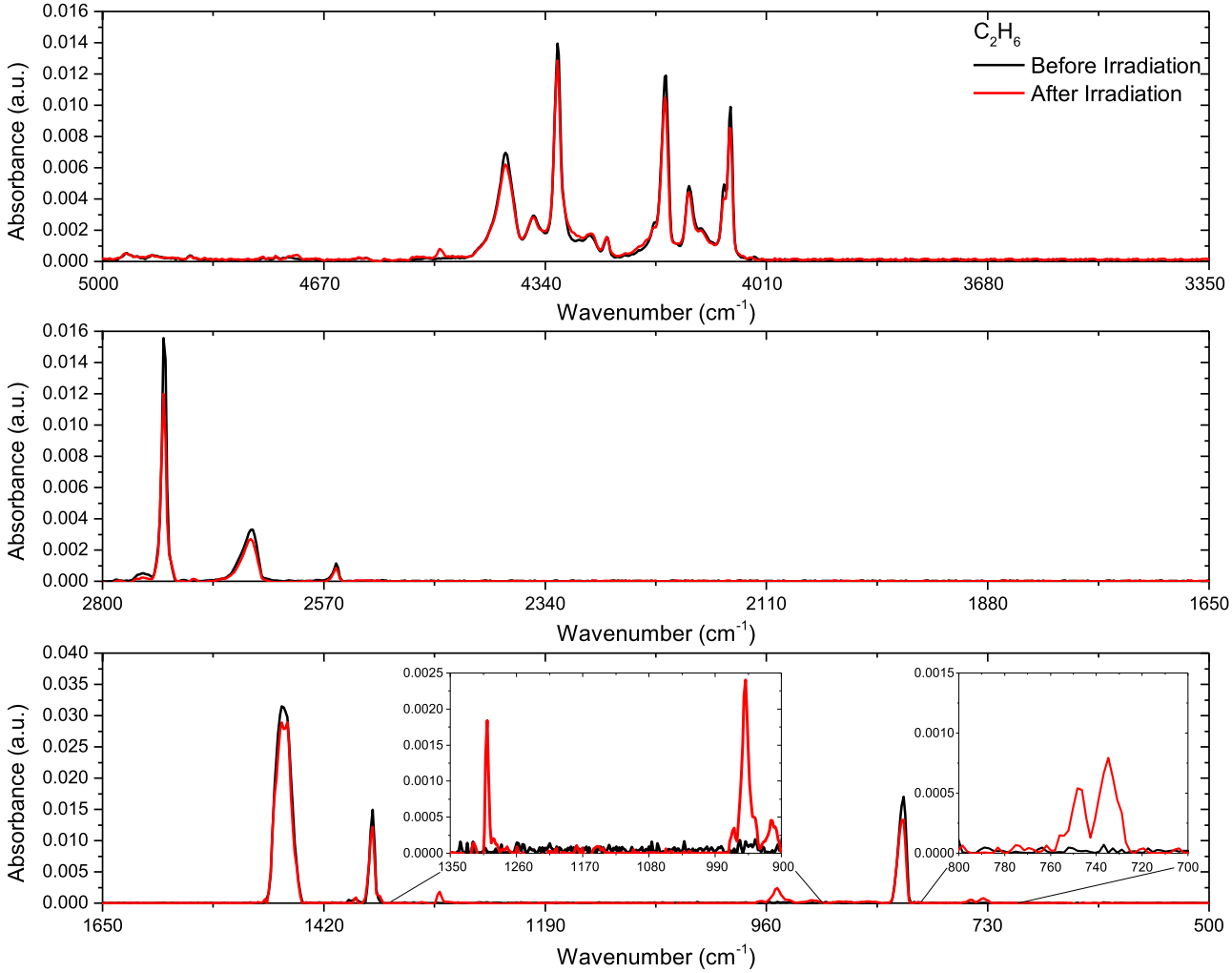

Figure 2. Infrared spectra for ethane (C_2H_6) before (black, dotted line) and after (red line) irradiation from 5000–3350 cm^{-1} (top), 2800–1650 cm^{-1} (middle), and 1650–500 cm^{-1} (bottom); assignments of the spectra are given in Table 1(a).

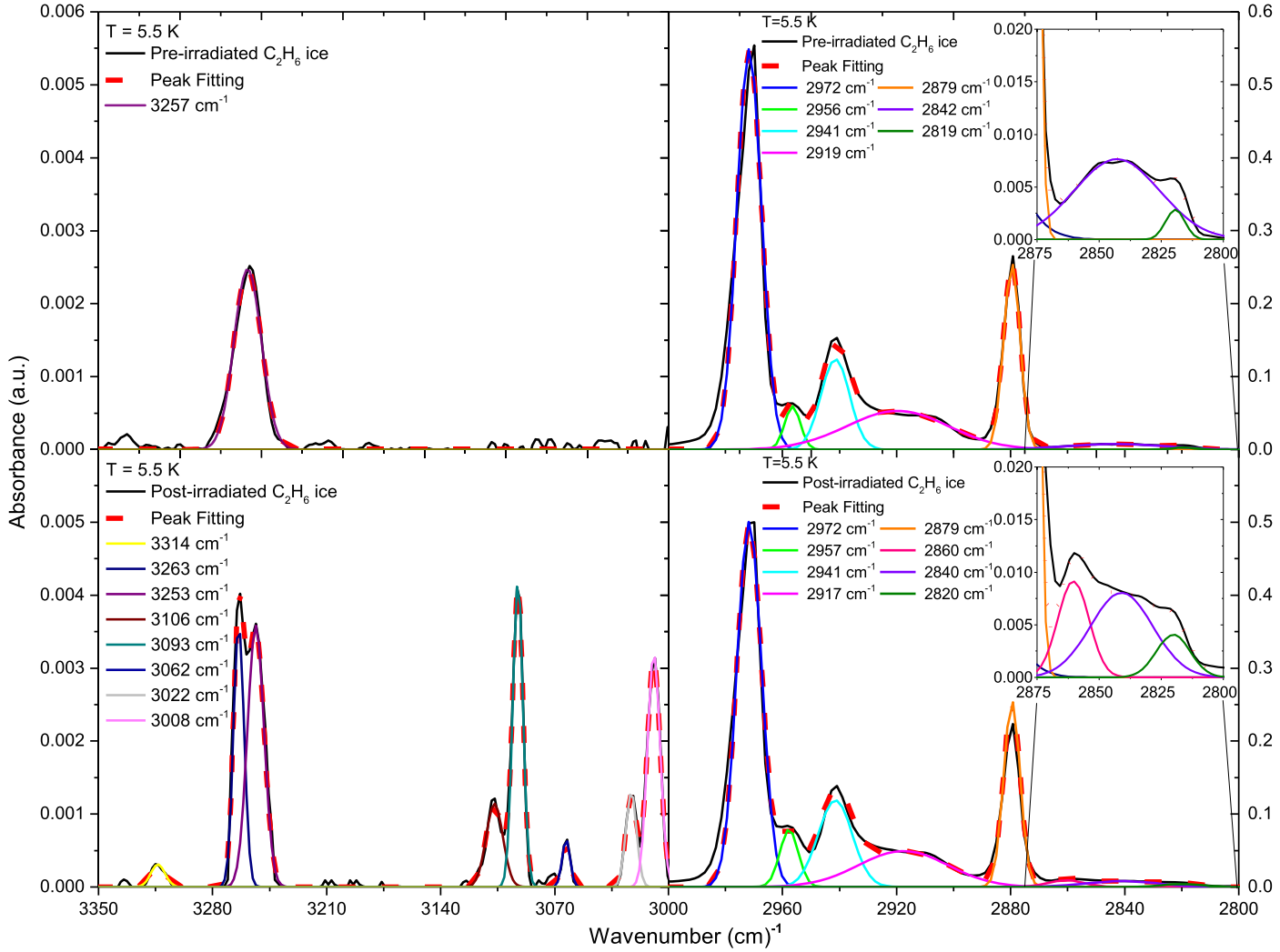

Figure 3. Deconvoluted infrared spectra of ethane (C_2H_6) from 3350–2800 cm^{-1} before (top panels) and after (bottom panels) the irradiation. The left side panels are zoomed by a factor of 100; assignments of the complete spectra are given in Table 1.

Here, exploiting PI-ReTOF-MS, we report the detection of complex hydrocarbon molecules from C_3 to C_{12}. Abplanalp et al. (2016) recently unveiled a much more complex chemistry taking place within the ices than previously reported (Jones & Kaiser 2013; Kaiser et al. 2014, 2015; Maity et al. 2015). The previous ethane irradiation analyses (FTIR, QMS, GC–MS) were only able to determine that hydrocarbons as large as butane isomers (C_4H_{10}) were produced from ethane irradiation. However, this was based on FTIR spectroscopy which, once more, is not very useful for this system as essentially all of the products will have overlapping group frequencies. However, the coupling of FTIR with PI-ReTOF-MS allows for much more detailed information to be extracted because after butane is observed to sublime, several infrared peaks still remain and their change in infrared intensities can be correlated with larger molecular weight hydrocarbons subliming during TPD. The analysis of pure ethane ice, after processing, with PI-ReTOF-MS is not only useful for determining the chemical pathways available within this simple hydrocarbon, but also crucial to fully understanding the processes available and taking place in any ice mixture that contains ethane. Although ethane remains to be detected in the interstellar medium (ISM), the detection of this molecule on comets, which are records of interstellar clouds, shows that it is likely that ethane does exist in the ISM (Mumma et al. 1996). This link of cometary ethane to an interstellar origin is crucial as comets represent the inventory of starting materials for the objects within our solar system and other star systems.

2. EXPERIMENTAL DETAILS

All experiments were executed in an ultrahigh vacuum (UHV) chamber that was evacuated to typically 3×10^{-11} torr (Kaiser et al. 2014). A cold finger, made from oxygen-free high conductivity copper connected to a UHV-compatible closed-cycle helium refrigerator (Sumitomo Heavy Industries, RDK-415E) was interfaced to the chamber using a UHV-compatible bellow (McAllister, BLT106) and a differentially pumped rotary feedthrough (Thermoionics Vacuum Products, RNN-600/FA/MCO) that allows it to be rotated in the horizontal plane or translated in the vertical plane, respectively. Interfaced to the cold finger via indium foil to ensure thermal conductivity, was a silver mirror, which acted as the substrate. A

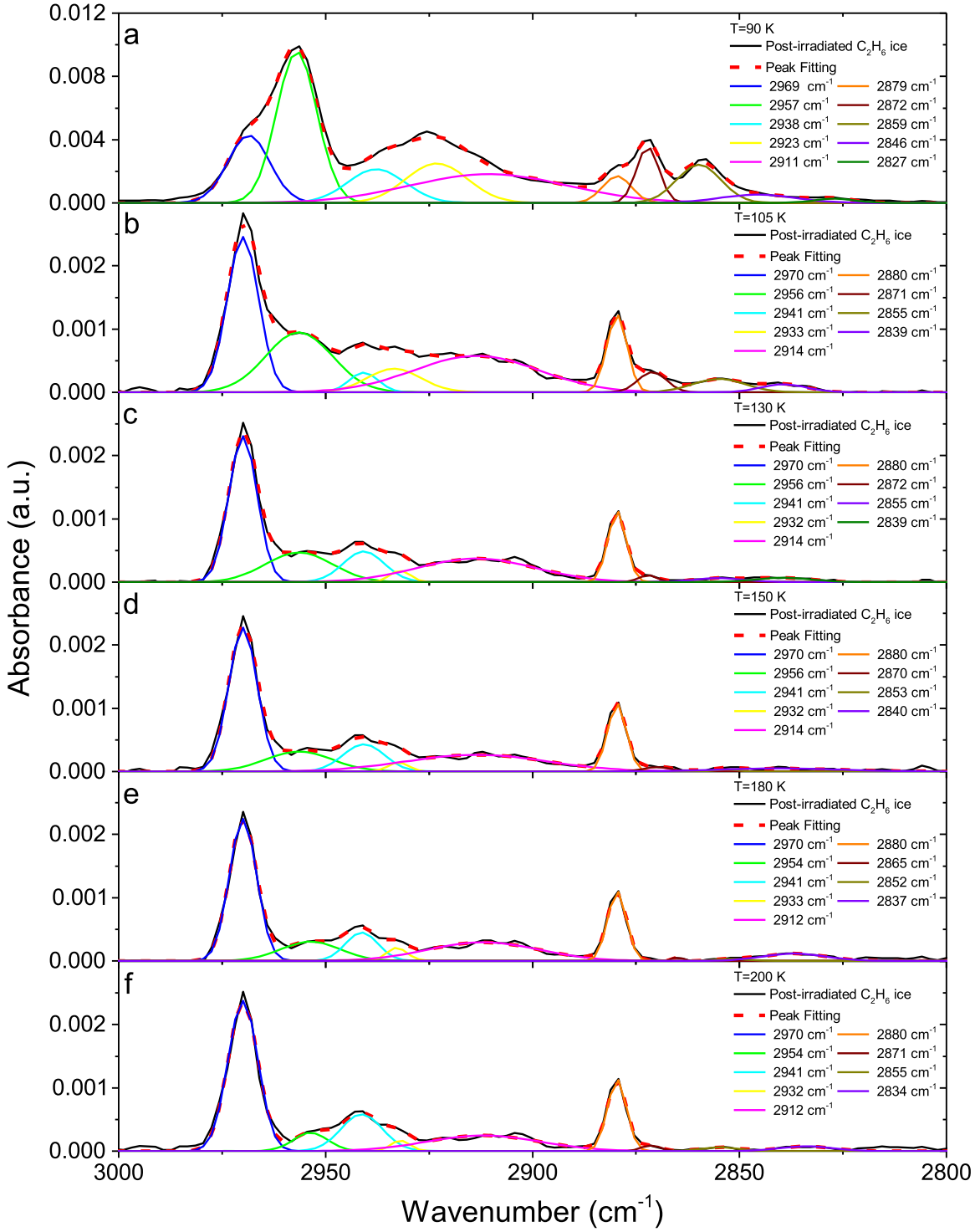

Figure 4. Deconvoluted infrared spectra of ethane (C_2H_6) from 3000–2800 cm^{-1} for selected temperatures corresponding to the sublimation temperatures of alkanes as observed via PI-ReTOF-MS.

glass capillary array was used to introduce the gases into the main chamber and was located about 30 mm away from the silver target. Typical pressures of 5×10^{-8} torr held for a few minutes resulted in the desired thickness of ice to be deposited: the ice thickness was determined in situ by using a refractive index (n) of $n = 1.34$ (Hudson et al. 2014) and monitoring, online and in situ, the interference pattern produced during the gas deposition via a HeNe laser ($\lambda = 632.8$ nm; CVI Melles-Griot; 25-LHP-230) reflecting off of the silver substrate into a photodiode (Groner et al. 1973; Maity et al. 2014a). The ice thickness was determined to be 475 ± 25 nm using this method. Using a modified Lambert–Beer relationship with absorption coefficients of 3.81×10^{-18}, 2.20×10^{-17}, 1.55×10^{-19}, 2.38×10^{-19}, and 2.18×10^{-19} cm molecule^{-1} (Hudson et al. 2014) and integrated areas for the respective infrared bands 2882 (ν_5), 2974 (ν_{10}), 4070

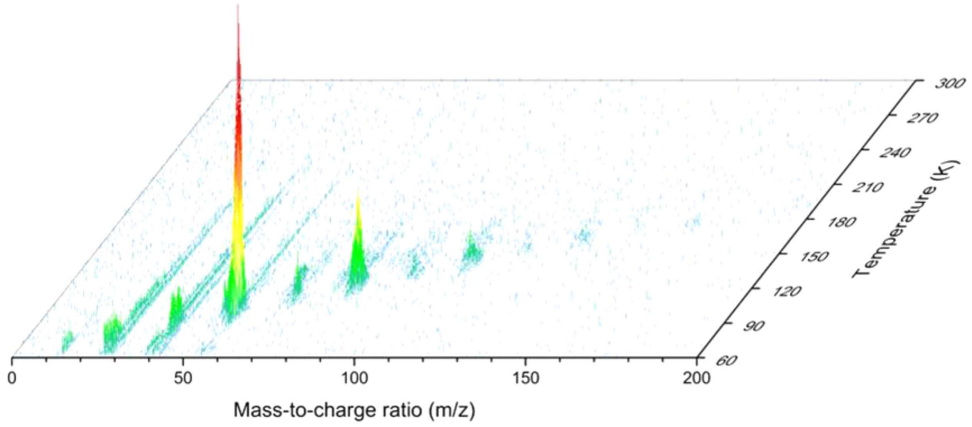

Figure 5. Recorded PI-ReTOF-MS data reporting the temperature dependent mass spectra for ethane (C_2H_6) at a photoionization energy of 10.49 eV.

Table 2
Masses Correlated to Molecules Detected in Both Experiments

m/z	C_2H_6 (30 nA; 10.49 eV)	C_2D_6 (30 nA; 10.49 eV)	m/z
40	C_3H_4	C_3D_4	44
42	C_3H_6	C_3D_6	48
52	C_4H_4	C_4D_4	56
54	C_4H_6	C_4D_6	60
56	C_4H_8	C_4D_8	64
57	$^{13}CC_3H_8$	$^{13}CC_3D_8$	65
58	C_4H_{10}	C_4D_{10}	68
66	C_5H_6	C_5D_6	72
67	$^{*}C_5H_7$	$^{*}C_5D_7$	74
68	C_5H_8	C_5D_8	76
69	$^{13}CC_4H_8$	$^{13}CC_4D_8$	77
70	C_5H_{10}	C_5D_{10}	80
79	$^{*}C_6H_7$	$^{*}C_6D_7$	86
80	C_6H_8	C_6D_8	88
81	$^{*}C_6H_9$	$^{*}C_6D_9$	90
82	C_6H_{10}	C_6D_{10}	92
84	C_6H_{12}	C_6D_{12}	96
86	C_6H_{14}	C_6D_{14}	100
93	$^{*}C_7H_9$	$^{*}C_7D_9$	102
95	$^{*}C_7H_{11}$	$^{*}C_7D_{11}$	106
96	C_7H_{12}	C_7D_{12}	108
98	C_7H_{14}	C_7D_{14}	112
110	C_8H_{14}	C_8D_{14}	124
112	C_8H_{16}	C_8D_{16}	128
114	C_8H_{18}	C_8D_{18}	132
124	C_9H_{16}	C_9D_{16}	140
126	C_9H_{18}	C_9D_{18}	144
138	$C_{10}H_{18}$	$C_{10}D_{18}$	156
140	$C_{10}H_{20}$	$C_{10}D_{20}$	160
142	$C_{10}H_{22}$	$C_{10}D_{22}$	164
	...	$C_{11}D_{20}/C_{12}D_{14}/C_{13}D_8/C_{14}D_2$	172
	...	$C_{11}D_{22}/C_{12}D_{16}/C_{13}D_{10}/C_{14}D_4$	176
	...	$C_{12}D_{20}/C_{13}D_{14}/C_{14}D_8/C_{15}D_2$	184
	...	$C_{12}D_{22}/C_{13}D_{16}/C_{14}D_{10}/C_{15}D_4$	188
	...	$C_{12}D_{24}/C_{13}D_{18}/C_{14}D_{12}/C_{15}D_6$	192

Note. Italicized formulae were only detected in the deuterated experiments, most likely due to a higher signal intensity of all products (see the text); * indicates a fragment.

($\nu_5 + \nu_{12}$), 4161 ($\nu_7 + \nu_{12}$), and 4321 ($\nu_6 + \nu_{10}$) yielded an average thickness of 440 ± 130 nm showing an agreement with the more accurate laser interferometry method. Isotopic ices of D6-ethane (C_2D_6, C.D.N. isotopes, >99% D) were also irradiated to confirm infrared assignments via isotopic shifts as well as aid in the identification of subliming molecules by their shift in mass-to-charge ratios.

After each ice had been deposited, it was continuously monitored in situ before, during, and after processing via a Fourier transform infrared spectrometer (Nicolet 6700), which probes the infrared active vibrational modes of the reactant and newly formed molecules within the sample. The FTIR recorded data in absorption–reflection–absorption mode at a reflection angle of 45° from 5000 to 500 cm^{-1} with a resolution of 4 cm^{-1}, which allowed for 30 spectra to be collected during the 1 hr of irradiation with 5 keV electrons. Once the irradiation was complete the ice was held at 5.5 K for 1 hr; thereafter TPD studies were conducted by heating the substrate to 300 K at a rate of 0.5 K $minute^{-1}$. In detail, during irradiation, an area of 1.0 ± 0.1 cm^2 of the ethane ice was exposed to 5 keV electrons at an incidence angle of 70° relative to the surface normal of the mirror for 1 hr at a current of 30 nA. Using Monte Carlo simulations via CASINO 2.42 software (Drouin et al. 2007), it was determined that an average penetration depth of the 5 keV electrons was 310 ± 20 nm, which is less than the total thickness of the ice, therefore ensuring that no interactions are taking place between the silver substrate and the energetic electrons. The average dose deposited into the ethane ices was calculated to be 6.6 ± 1.7 eV $molecule^{-1}$ (21.2 MGy) utilizing a density of 0.719 g cm^{-3} (van Nes 1978).

During the TPD phase, the ice was monitored with FTIR and the subliming molecules were monitored via both a quadrupole mass spectrometer (EI-QMS; Extrel, Model 5221) and the PI-ReTOF-MS technique. The EI-QMS operates in a residual-gas analyzer (RGA) mode with the mass range from 1–300 amu with a 100 eV electron impact ionization source and an emission current of 1 mA. The details of PI-ReTOF-MS have previously been described (Jones & Kaiser 2013; Abplanalp et al. 2015); briefly, the technique consisted of first ionizing the subliming molecules via single-photon ionization by pulsed coherent VUV light with an energy of 10.49 eV (λ = 118.2 nm). The ionized molecules are detected utilizing a modified reflectron time-of-flight mass spectrometer (ReTOF; Jordan TOF Products, Inc.), and the ions are detected via a multichannel plate (MCP) in a dual chevron configuration. The MCP signal was amplified with a fast pre-amplifier (Ortec

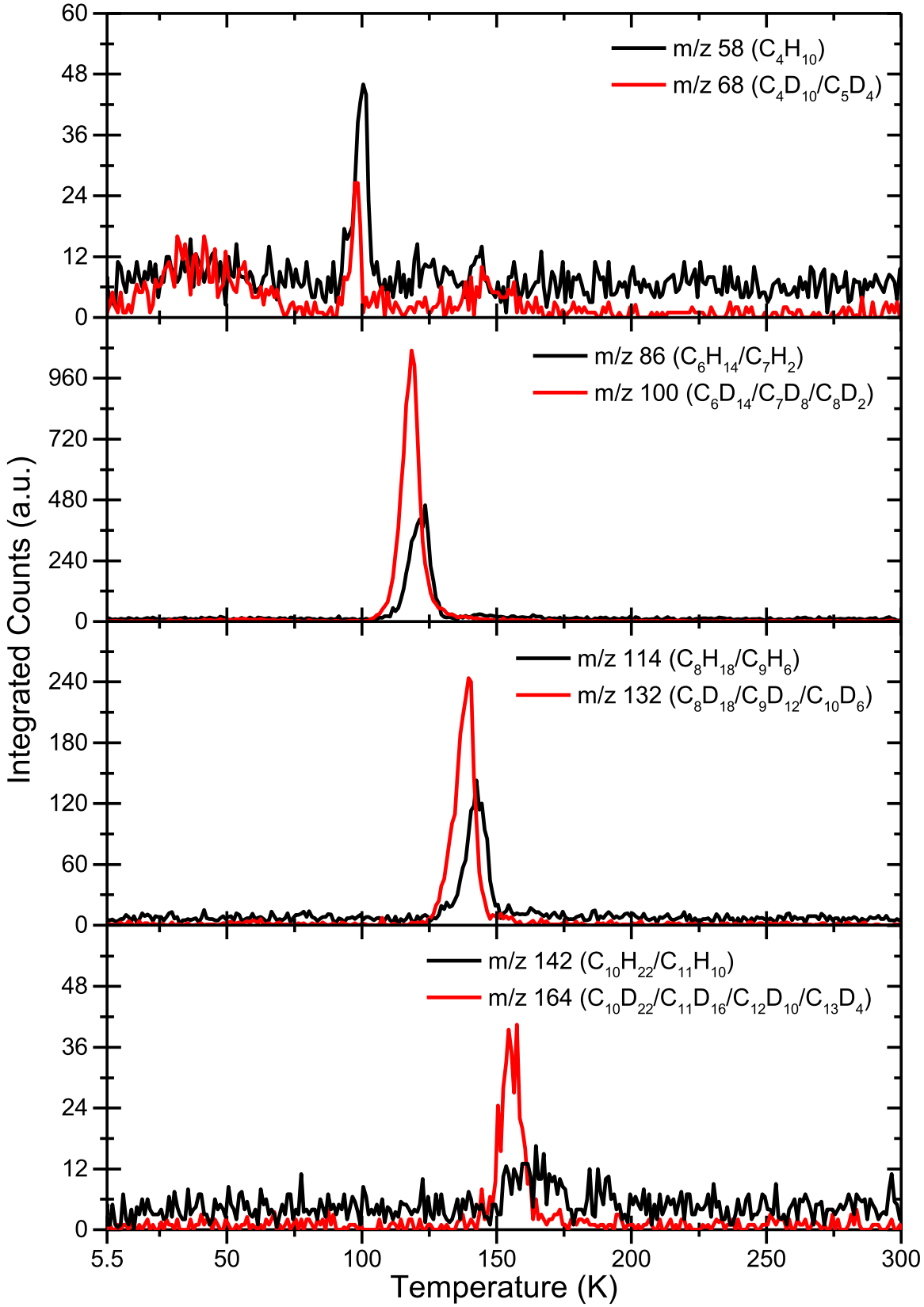

Figure 6. TPD profiles recorded via PI-ReTOF-MS for masses with the generic formula of C_nH_{2n+2}/C_nD_{2n+2} (alkanes). Note that only masses corresponding to an even number of carbon atoms being incorporated into the molecule are formed.

9305) and then shaped by a 100 MHz discriminator. These spectra were then recorded by a personal-computer-based multichannel scaler (FAST ComTec, P7888-1 E) using parameters of 4 ns bin width triggered at 30 Hz (Quantum Composers, 9518), 3600 sweeps in a mass spectrum per 1 K change in temperature of the substrate.

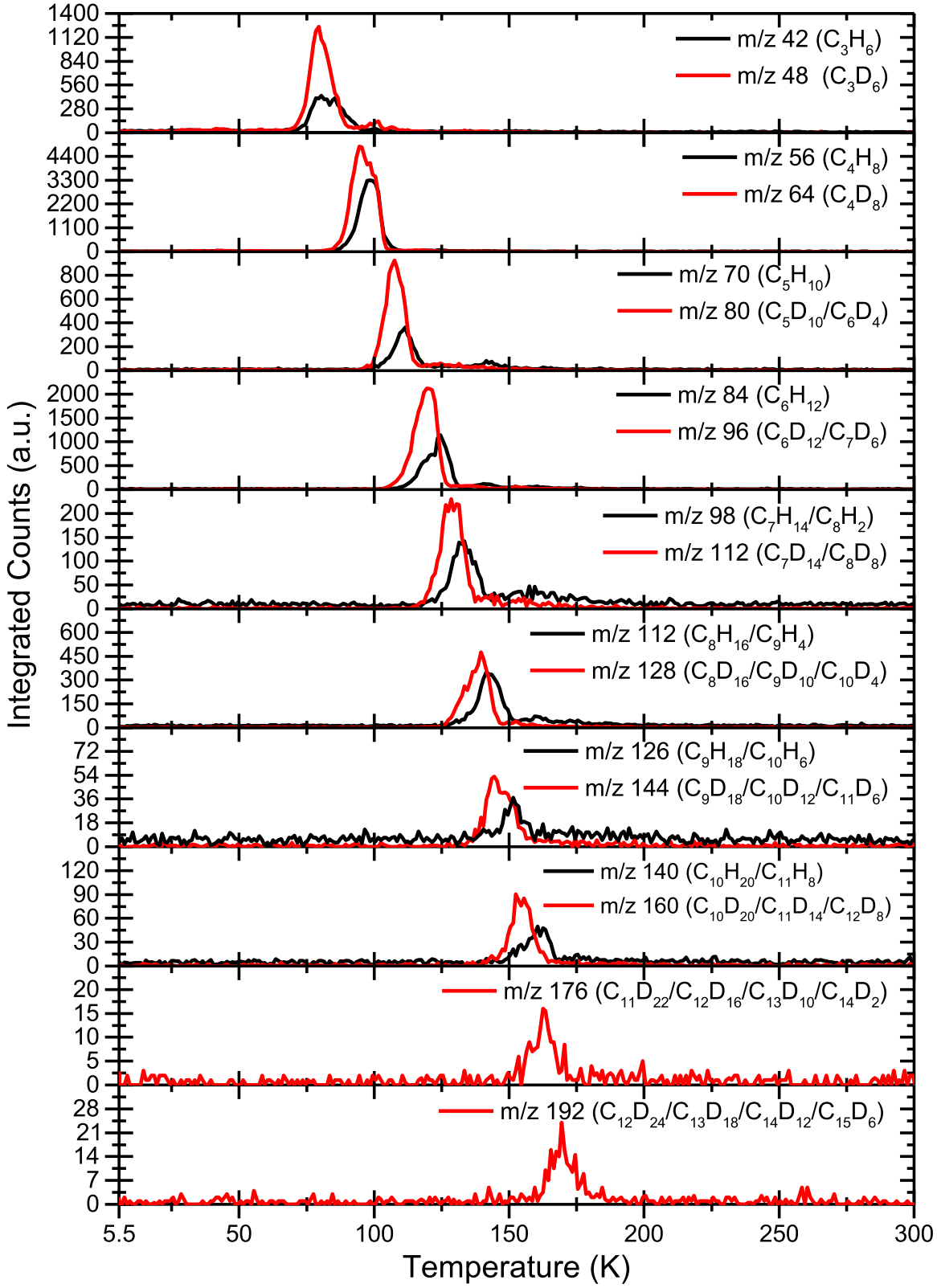

Figure 7. TPD profiles recorded via PI-ReTOF-MS for masses with the generic formula of C_nH_{2n}/C_nD_{2n}, which may correspond to alkenes and/or cycloalkanes.

3. RESULTS

3.1. Infrared Spectroscopy

The FTIR in situ analysis during the irradiation detected new infrared absorptions as well as the broadening of the ethane modes, suggesting that the fundamentals of (some of the) newly formed molecules may overlap with those of the reactants. Fundamentals corresponding to methane (CH_4), acetylene (C_2H_2), ethylene (C_2H_4), the ethyl radical (C_2H_5), 1-butene (C_4H_8), and *n*-butane (C_4H_{10}) were assigned in both the ethane (Table 1(a), Figure 1) and D6-ethane ices (Appendix A.1). The detection of 1-butene and *n*-butane, but not their

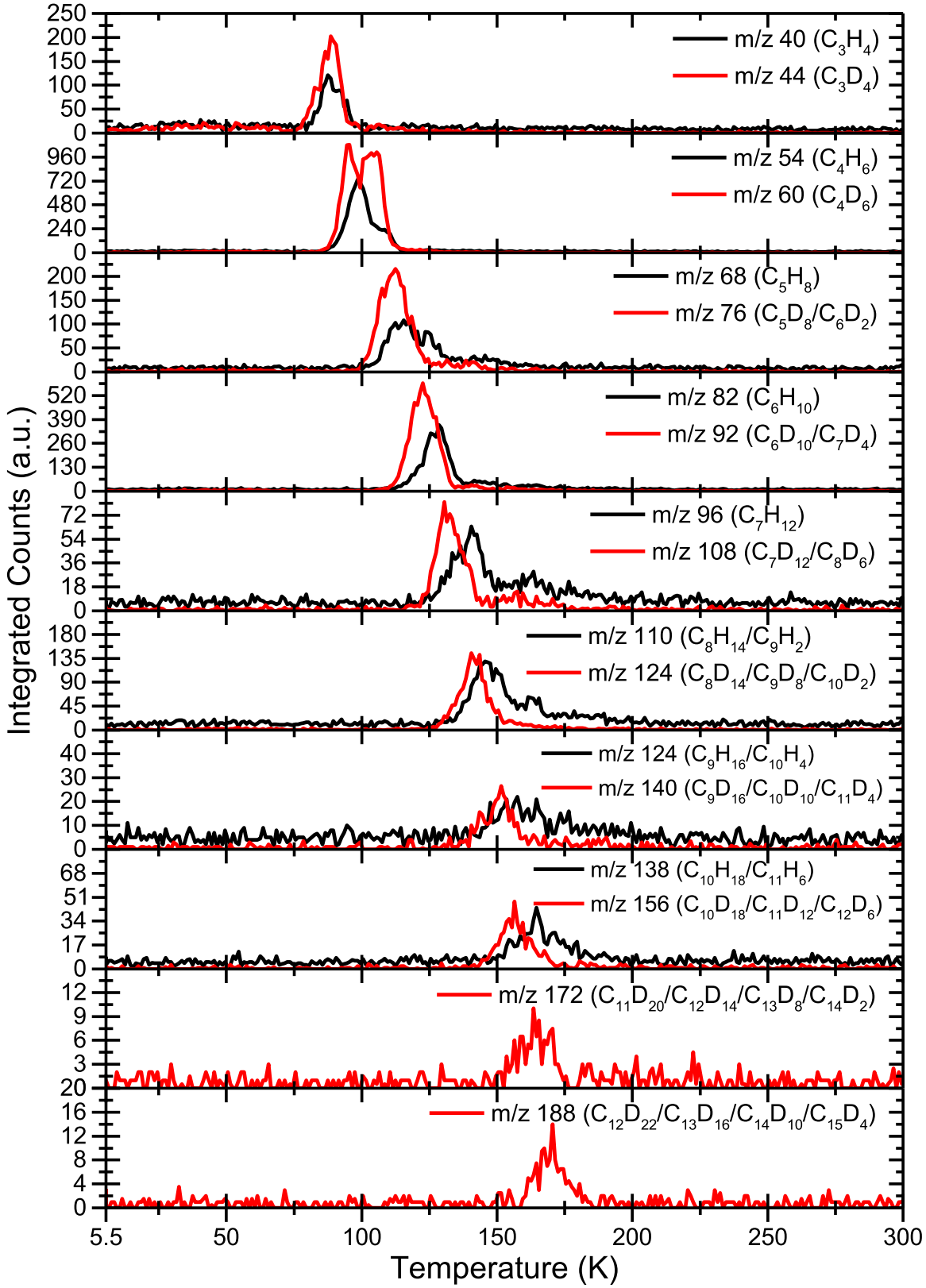

Figure 8. TPD profiles recorded via PI-ReTOF-MS for masses with the generic formula of C_nH_{2n-2}/C_nD_{2n-2}, which may correspond to alkynes, dienes, and/or cycloalkenes.

isomers, is in agreement with previous studies (Jackson et al. 1966; Hudson et al. 2009; Kim et al. 2010) and reaffirms the proposed reaction mechanism of two ethyl radicals forming *n*-butane followed by dehydrogenation to 1-butene (Section 4). Figure 2 shows that the absorptions in the spectrum from 5000–3350 cm^{-1} and 2800–500 cm^{-1} are easily assigned to the

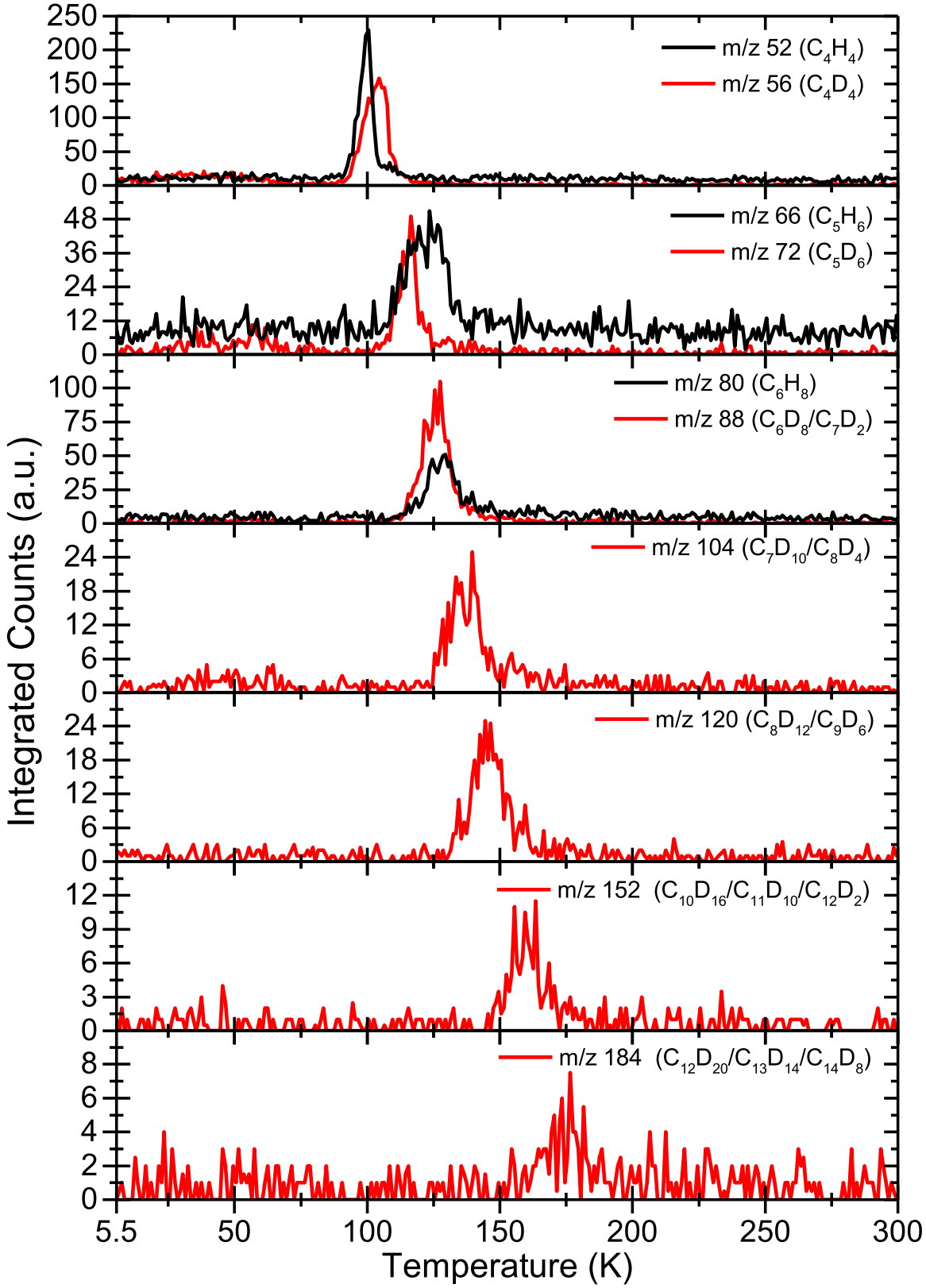

Figure 9. TPD profiles recorded via PI-ReTOF-MS for masses with the generic formula of C_nH_{2n-4}/C_nD_{2n-4} (yne-ene, trienes, cyclodialkenes, bicycloalkenes).

reactants and aforementioned products formed within the ethane ice upon irradiation. However, in the range of 3350–2800 cm^{-1} there are several new infrared features that appear in overlapping positions after the processing with energetic electrons (Figure 3). To determine the contributors to these bands, a deconvolution of the spectra, previously described (Kaiser et al. 2014; Abplanalp et al. 2015), was necessary. The deconvolution method showed that eight new

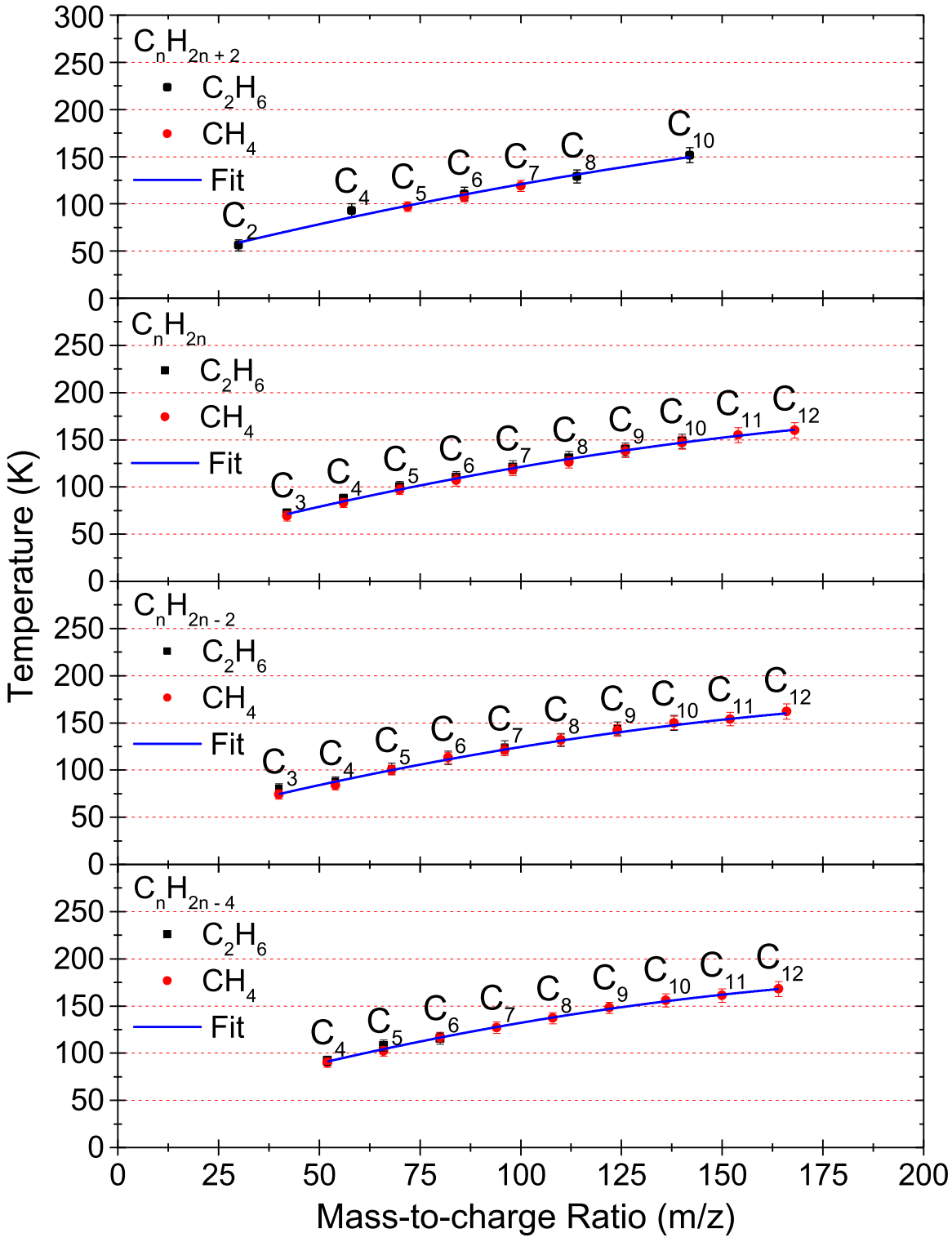

Figure 10. Sublimation onset temperatures of C_nH_{2n+2} (n = 4, 6, 8, 10), C_nH_{2n} (n = 3–10), C_nH_{2n-2} (n = 3–10), and C_nH_{2n-4} (n = 4–6). Black points are from irradiated ethane (C_2H_6) and red points are from irradiated methane (CH_4) ices from Jones & Kaiser (2013).

infrared stretches were identifiable beyond the reactants (Table 1). It is interesting to point out that the ethyl radical (C_2H_5) was observable in the infrared, but that there was no detection of the formation of the methyl radical. The implications of these observations are that ethane bond breaking occurs between carbon–hydrogen bonds but not carbon–carbon bonds (Section 4). These findings correlate well with results from previous studies examining the processing of ethane at astrophysically relevant temperatures; Kim et al. (2010) identified the largest molecule formed in the ices as *n*-butane via recombination of two ethyl radicals using FTIR spectroscopy.

During the TPD studies, the FTIR sampling of the ice shows evidence that higher molecular weight molecules beyond C4

Table 3
Data Applied to Calculate the Absorbed Dose per Molecule in C_2H_6 and C_2D_6 Ices

Initial kinetic energy of the electrons, E_{init}	5 keV
Irradiation current, I	30 ± 2 nA
Total number of electrons	$(6.7 \pm 0.5) \times 10^{14}$
Average kinetic energy of backscattered electrons, E_{bs} [a]	3.0 ± 0.3 keV
Fraction of backscattered electrons, f_{bs} [a]	0.28 ± 0.03
Average kinetic energy of transmitted electrons, E_{trans} [a]	1.6 ± 0.3 keV
Fraction of transmitted electrons, f_{trans} [a]	0.12 ± 0.01
Average penetration depth, l [a]	310 ± 20 nm
Density of the ice, ρ	0.719 ± 0.07 g cm^{-3}
Irradiated area, A	1.0 ± 0.1 cm^2
Total # molecules processed	$(4.5 \pm 1.2) \times 10^{17}$
Dose per 30 amu, D_{C2H6}	6.0 ± 1.1 eV
Dose per 36 amu, D_{C2D6}	7.1 ± 1.3 eV

Note.
[a] CASINO output values.

hydrocarbons are still present on the substrate at temperatures from 90 to 200 K (Figures 4(a)–(f)). Figure 4(a) presents the deconvoluted infrared spectrum from 3000–2800 cm^{-1} at 90 K, which is just before *n*-butane sublimes, while Figure 4(b) depicts the spectral range at 105 K, after butane has sublimed. According to the FTIR assignments, there are several infrared stretches from 3000–2800 cm^{-1} that remain beyond 200 K. Therefore, it is likely that larger molecular weight compounds were formed in the irradiation of the ethane ice (Sections 3.2 and 3.3). The dual analysis of the system via FTIR and mass spectrometry (RGA and PI-ReTOF-MS) during the TPD allows for further analysis as a decline in the infrared spectrum with the concurrent detection of a subliming molecule can be correlated.

3.2. Mass Spectrometry—RGA

During the TPD phase of the experiment the subliming molecules are monitored via two mass spectrometric techniques (RGA; PI-ReTOF-MS). Although the RGA represents the less sensitive technique (Turner et al. 2015), it is useful for detecting molecules that have ionization energies above 10.49 eV. Due to the RGA utilizing an electron impact (100 eV) ionizer, the ion counts detected often result from dissociative ionization. Therefore, only alkanes were able to be identified explicitly since their parent ions cannot originate from dissociative electron impact ionization of higher molecular weight species (Appendix A.2).

3.3. Mass Spectrometry—PI-ReTOF-MS

The analyses of the subliming molecules from the irradiated ethane ice via PI-ReTOF-MS utilizing 10.49 eV photons are summarized in Figure 5 and Table 2 (Appendix A.3). Figure 5 shows the intensity of ions as a function of temperature for the irradiated ethane (C_2H_6) ices with detected mass-to-charge ratio signals close to $m/z = 200$. Four specific groups of molecules using the following general molecular formulae were detected: C_nH_{2n+2} (n = 4, 6, 8, 10), C_nH_{2n} (n = 3–10), C_nH_{2n-2} (n = 3–10), and C_nH_{2n-4} (n = 4–6) (Figures 6–9). These four groups were found to contain many ions that correspond to molecules never before detected in ethane irradiation experiments, and these data reveal several interesting trends previously unobserved.

3.3.1. C_nH_{2n+2}

The mass-to-charge ratios corresponding to the alkanes (C_nH_{2n+2}) of n = 4, 6, 8, 10 were detected using PI-ReTOF-MS (Figure 6). Both the methane (CH_4) and propane (C_3H_8) products could not be detected via PI-ReTOF-MS since their ionization energies of 12.61 eV and 10.94 eV (Lias et al. 2016), respectively, are higher than the 10.49 eV used in the present experiments. The molecular ion of *n*-butane, which agrees with the FTIR analysis and previous experiments (Hudson et al. 2009; Kim et al. 2010), was identified via $m/z = 58$ ($C_4H_{10}^+$) with a sublimation onset at 93 K. However, larger alkanes were also detected at $m/z = 86$ ($C_6H_{14}^+$, 111 K), $m/z = 114$ ($C_8H_{18}^+$, 129 K), and $m/z = 142$ ($C_{10}H_{22}^+$, 152 K). This corresponds to an increase in sublimation temperature by 13–18 K per C_2H_4 unit added. Figure 10 displays this interesting trend of an increasing sublimation temperature as the molecular weight rises, not only for alkanes, but for each group of hydrocarbons that were detected. The signal intensity of $m/z = 58$ ($C_4H_{10}^+$) is quite low, which is most likely due to the ionization energy of *n*-butane ($CH_3CH_2CH_2CH_3$; 10.5 ± 0.1 eV) (Lias 1982, p. 409) being at the threshold of the photoionization energy used in these experiments (10.49 eV).

3.3.2. C_nH_{2n}

Observed alkenes (C_nH_{2n}) or the double-bond equivalent (D.B.E.) (cycloalkanes) of n = 3–10 were probed as well (Figure 7). As expected from the FTIR analysis, the molecular ion corresponding to butenes was observed at $m/z = 56$ ($C_4H_8^+$) with a sublimation onset of 88 K. Similarly to the alkanes observed, multiple hydrogen-deficient hydrocarbons were detected at $m/z = 42$ ($C_3H_6^+$, 72 K), $m/z = 70$ ($C_5H_{10}^+$, 100 K), $m/z = 84$ ($C_6H_{12}^+$, 111 K), $m/z = 98$ ($C_7H_{14}^+$, 121 K), $m/z = 112$ ($C_8H_{16}^+$, 131 K), $m/z = 126$ ($C_9H_{18}^+$, 140 K), and $m/z = 142$ ($C_{10}H_{20}^+$, 149 K), i.e., an increase of the sublimation temperature of typically 9–16 K per CH_2 unit. Similarly to the C_nH_{2n+2n} group the signal intensity decreases with increasing molecular size. Interestingly, this trend is separated based on even and odd carbon units in the ions. To clarify, a decrease in signal is not observed from an odd carbon ion ($C_3H_6^+$) to an even carbon ion ($C_4H_8^+$), but a decrease in signal from the smallest odd carbon ion ($C_3H_6^+$) to the next largest odd carbon ion ($C_5H_{10}^+$) shows a consistent trend through to the largest odd carbon ion ($C_9H_{18}^+$). Likewise the trend is monitored from the smallest even carbon ion ($C_4H_8^+$) to the largest even carbon ion ($C_{10}H_{20}^+$). Overall, the intensities of the odd carbon ions ($C_3H_6^+$, $C_5H_{10}^+$, $C_7H_{14}^+$, $C_9H_{18}^+$) are lower than the signal intensities for the even carbon ions ($C_4H_8^+$, $C_6H_{12}^+$, $C_8H_{16}^+$, $C_{10}H_{20}^+$) of similar size. This difference in signal intensity between the even and odd constituents detected may be due to the formation mechanism, which is discussed in Section 4.7 and suggests that the alkanes, all of which had even carbon units, are formed first and desaturation/degradation of these produces the other detected molecules in the present experiment. However, as previously stated, each isomer must be uniquely detected in order to comment on the relative quantity produced based on their individual photoionization cross sections.

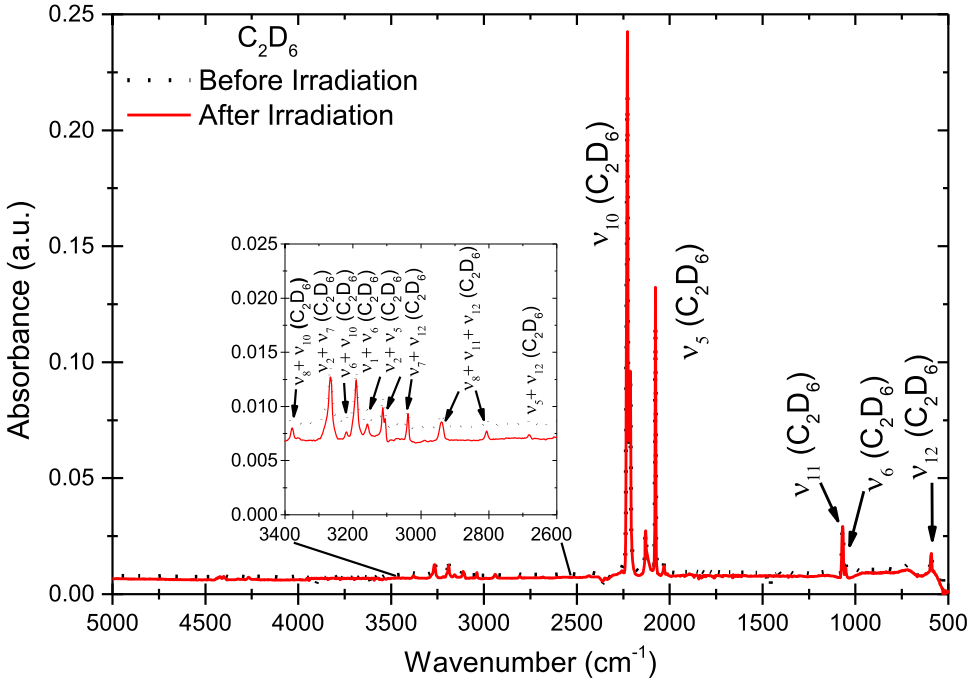

Figure 11. Infrared spectra from 5000 to 500 cm^{-1} for D6-ethane (C_2D_6; bottom) ices before (black, dotted line) and after (red, solid line) the irradiation with a tenfold zoom of the overtones in the inset box along with assignments (Table 1(b)).

3.3.3. C_nH_{2n-2}

Although the FTIR analysis was not able to determine the presence of any alkynes larger than acetylene, several mass-to-charge ratios corresponding to alkynes (C_nH_{2n-2}) or the triple-bond equivalent (T.B.E.) (dienes, cycloalkenes, bicycloalkanes) of $n = 3$–10 were identified (Figure 8). These ions were observed at $m/z = 40$ ($C_3H_4^+$, 81 K), $m/z = 54$ ($C_4H_6^+$, 88 K), $m/z = 68$ ($C_5H_8^+$, 102 K), $m/z = 82$ ($C_6H_{10}^+$, 113 K), $m/z = 96$ ($C_7H_{12}^+$, 124 K), $m/z = 110$ ($C_8H_{14}^+$, 132 K), $m/z = 124$ ($C_9H_{16}^+$, 144 K), and $m/z = 138$ ($C_{10}H_{18}^+$, 150 K). With each additional CH_2 unit, an increase in sublimation temperature by 6–12 K was observed. This hydrocarbon group follows an identical trend to the C_nH_{2n} group in that signal decreases with increasing size based on even or odd carbon units contained in the detected ion.

3.3.4. C_nH_{2n-4}

The last group of hydrocarbons detected corresponded to C_nH_{2n-4}, which has several different molecular structures (yne-ene, trienes, cyclodialkenes, bicycloalkenes) of $n = 4$–6 (Figure 9). These ions were observed at $m/z = 52$ ($C_4H_4^+$, 92 K), $m/z = 66$ ($C_5H_6^+$, 108 K), and $m/z = 80$ ($C_6H_8^+$, 116 K). Each additional CH_2 unit resulted in an increase in sublimation temperature by 8–16 K for this hydrocarbon group. This group represents the most highly unsaturated molecules detected in this experiment and a group that was previously undetected in prior experiments (Scheer et al. 1962; Jackson et al. 1966; Hudson et al. 2009; Kim et al. 2010).

3.3.5. Other Masses: Fragments and Isotopes

Several other ions were also detected, including $m/z = 57$, $m/z = 67$, $m/z = 69$, $m/z = 79$, $m/z = 81$, $m/z = 93$, and $m/z = 95$. However, each of these ions is explainable by either natural ^{13}C-isotopic abundances or fragmentation of larger hydrocarbons (Appendix A.4). It should be noted that several ions were only able to be detected in the deuterated experiments, most likely due to a difference in photon-flux during their detection. These were first observed in the C_nH_{2n} group for C11 and C12 molecules and are also detected in the C_nH_{2n-2} system for C11 and C12 molecules following the proposed trend closely (Figure 10). In the C_nH_{2n-4} group C7, C8, C10, and C12 molecules were tentatively detected, but no cross analysis was possible.

4. DISCUSSION

4.1. Compilation of Data Analysis

Before we move on to the discussion, we would like to compile the experimental results. This will assist in the derivation of the reaction mechanism and placing the data into astrophysical context.

1. The infrared spectroscopic investigation only detected six C1 to C4 hydrocarbons: methane (CH_4), acetylene (C_2H_2), ethylene (C_2H_4), the ethyl radical (C_2H_5), 1-butene (C_4H_8), and *n*-butane (C_4H_{10}).
2. The EI-QMS data provide evidence on the formation of two alkanes: propane (C_3H_8) and butane (C_4H_{10}).
3. The PI-ReTOF-MS investigation revealed four groups with a total of 23 hydrocarbon molecules. These are in increasing order of degrees of desaturation: C_nH_{2n+2} ($n =$ 4, 6, 8, 10), C_nH_{2n} ($n = 3$–10), C_nH_{2n-2} ($n = 3$–10), and C_nH_{2n-4} ($n = 4$–6).

4.2. C_nH_{2n+2}

The ions corresponding to alkanes (C_nH_{2n+2}) of $n = 4$, 6, 8, and 10 were detected using PI-ReTOF-MS (Figure 6); these ions can only correspond to alkanes. First, it is very interesting that the only alkanes detected—with the exception of propane (C_3H_8) monitored via EI-QMS (Appendix A.2)—contained an

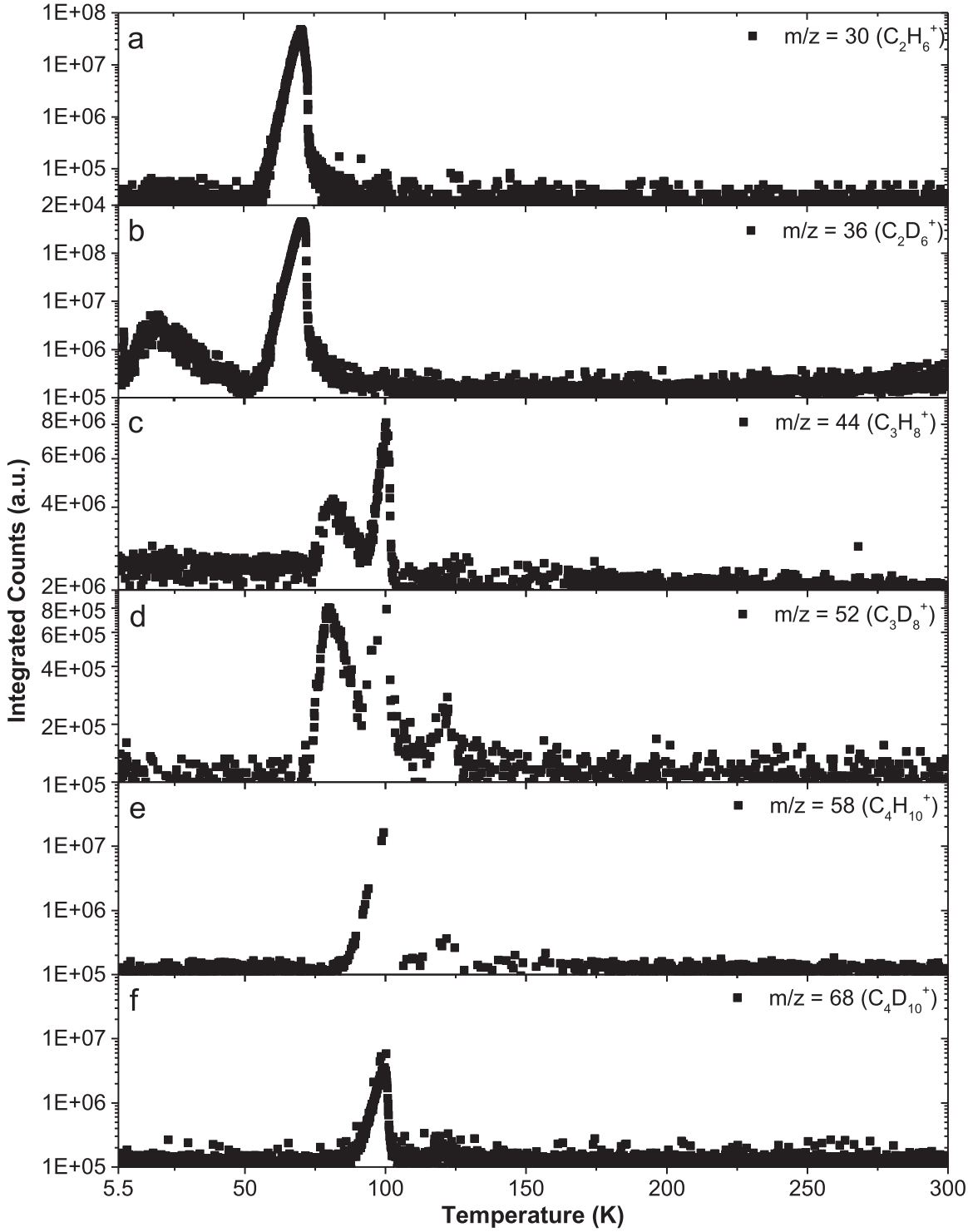

Figure 12. TPD profiles recorded during temperature programmed desorption via the RGA for ethane (C_2H_6/C_2D_6), propane (C_3H_8/C_3D_8), and butane (C_4H_{10}/C_4D_{10}).

even number of carbon atoms (C_4H_{10}, C_6H_{14}, C_8H_{18}, $C_{10}H_{22}$). With previous experiments only detecting alkanes as large as butane, this observation was not possible (Scheer et al. 1962; Jackson et al. 1966; Hudson et al. 2009; Kim et al. 2010). With the exception of C_4H_{10}, which can be only the straight chain isomer considering the ionization energies, the single experiment at 10.49 eV does not discriminate between the structural isomers explicitly. The detection of these even carbon chain alkanes reinforces the FTIR observation that only ethyl radicals (C_2H_5) were observed, but not methyl (CH_3) radicals, and suggests that the ethyl radical represents a key element to build up the alkanes via molecular C2 building blocks (Section 4.7). Previous experiments irradiating methane also detected large ions attributable to alkanes as large as heptane (C_7H_{16}) (Jones & Kaiser 2013) and dodecane ($C_{12}H_{26}$) (Kaiser et al. 1992), which revealed that alkanes have been a major source of

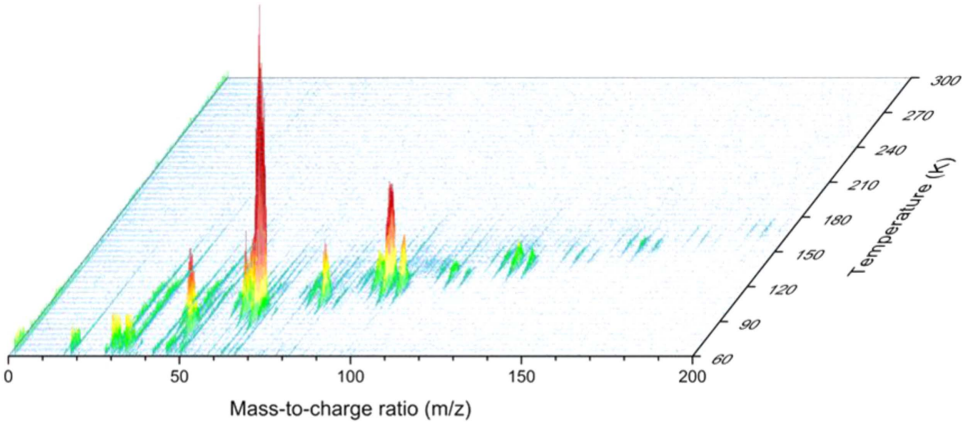

Figure 13. Recorded PI-ReTOF-MS data reporting the temperature-dependent mass spectra for D6-ethane (C_2D_6) at a photoionization energy of 10.49 eV.

interest and knowledge to the astrochemistry community. Alkanes provide clues to link comets and meteorites to an interstellar origin based on their similar chemical compositions (see Section 5). As previously stated, butane was also detected via the EI-QMS, the largest alkane detected by this method, and the sublimation temperatures correlate nicely between the two mass spectrometry methods. It should also be mentioned that the only alkane containing an odd number of carbons was propane (C_3H_8) (Appendix A.2). The ionization energy of propane is 10.9 ± 0.1 eV (Bieri et al. 1977), which is larger than the photoionization energy used in this PI-ReTOF-MS study, and therefore would not be detectable if it were produced.

4.3. C_nH_{2n}

Observed alkenes (C_nH_{2n}) or their D.B.E.s (cycloalkanes) of n = 3–10 were detected using PI-ReTOF-MS (Figure 7). An interesting difference between the alkane group and this group is that an odd number of carbons are now also incorporated in the molecules detected for the C_nH_{2n} group (n = 3–10; Section 4.6). The detection of C_3H_6 is interesting as the propylene isomer (CH_2CHCH_3; IE = 9.73 eV) has been observed in the ISM toward TMC-1 (Marcelino et al. 2007; Rawlings et al. 2013; Zhou et al. 2013). The second C_3H_6 isomer, cyclopropane (IE = 9.86 eV), represents the simplest cycloalkane. However, the confirmation of which C_3H_6 isomers are formed will require a discrimination of the isomers based on their ionization energies exploiting tunable VUV light to ionize the subliming molecules (Abplanalp et al. 2015). As observed by FTIR spectroscopy, the generation of 1-butene (C_4H_8; IE = 9.55 eV) was previously observed (Kim et al. 2010) in the processing of ethane ice. Dartois et al. (2005) conducted a UV photolysis of trans-2-butene and showed the formation of a carbon polymer. Several alkenes (n = 2–6) were studied using theoretical models in an attempt to replicate gas phase reactions possibly taking place in Titan's atmosphere (Woon & Park 2009), revealing that there is a tendency to produce multiple unsaturated bonds upon exposure to ionizing radiation. Pilling et al. (2012) experimentally studied the irradiation of cyclohexane (c-C_6H_{12}) with 219 MeV $^{16}O^{7+}$ and 632 MeV $^{58}Ni^{24+}$ ions and determined that production of unsaturated molecules takes place. Cyclodecane ($C_{10}H_{20}$) reactions with PAHs were previously studied as well and determined that photoalkylation occurred during UV processing under ISM conditions (Mahajan et al. 2002).

4.4. C_nH_{2n-2}

Mass-to-charge ratios corresponding to alkynes (C_nH_{2n-2}) or their T.B.E. (dienes, cycloalkenes, bicycloalkanes) of n = 3–10 were also identified (Figure 8). With previous experiments (Scheer et al. 1962; Jackson et al. 1966; Kim et al. 2010) achieving the detection of only C_4H_{10} (C_nH_{2n+2}) and C_4H_8 (C_nH_{2n}), the detection of C_3H_4 determined that higher order unsaturated groups were also produced conforming to alkynes or their T.B.E. (C_nH_{2n-2}). The C_nH_{2n-2} group showed an identical trend to the C_nH_{2n} group by incorporating an odd number of carbons in the molecules detected (n = 3–10). The C_3H_4 isomer methylacetylene (CH_3CCH; IE = 10.36 eV) isomer has been detected in a few astronomical surveys toward SgrB2, PKS 1830-211, L1544, and tentatively in NCG 4418 (Belloche et al. 2013; Muller et al. 2014; Vastel et al. 2014; Costagliola et al. 2015). Methylacetylene and its isomer allene (H_2CCCH_2; IE = 9.69 eV) have been reactants in attempts to untangle the chemistry taking place in Titan's atmosphere (Vakhtin et al. 2001; Goulay et al. 2007; Zhang et al. 2009).

Following the trend of the n-butane (C_4H_{10}) and 1-butene (C_4H_8) detection, C_4H_6 was also monitored. Four isomers exist; these are 1, 3-butadiene ($H_2CCHCHCH_2$; IE = 9.07 eV), 1, 2-butadiene ($H_2CCCH(CH_3)$; IE = 9.03 eV), 1-butyne ($HCCC_2H_5$; IE = 10.18 eV), and 2-butyne (CH_3CCCH_3; IE = 9.58 eV). The 1, 3-butadiene isomer represents a crucial building block in gas phase reactions with dicarbon (C_2) to form the phenyl radical (C_6H_5) (Zhang et al. 2010), and also with the tolyl radical ($C_6H_4CH_3$) forming 6-methyl-1, 4-dihydronaphthalene (Parker et al. 2014). Isoprene ($CH_2C(CH_3)CHCH_2$; IE = 8.86 eV) represents another interesting prospective molecule in this group, belonging to the C_5H_8 isomers, as it has been a key hydrocarbon in unraveling methyl-substituted PAH formation mechanisms (Dangi et al. 2014). Dartois et al. (2005) performed UV photolysis of solid 1, 5-hexadiene (C_6H_{10}), which resulted in the production of a carbonaceous polymer. Stephens & Bauer (1994) studied 2, 4-dimethyl-1, 3-pentadiene (C_7H_{12}) infrared emissions via shock heating in order to determine their contribution to PAH signatures.

4.5. C_nH_{2n-4}

Finally, we detected molecules corresponding to C_nH_{2n-4} that can have several different molecular connectivities (yne-ene, trienes, cyclodialkenes, bicycloalkenes) of n = 4–6

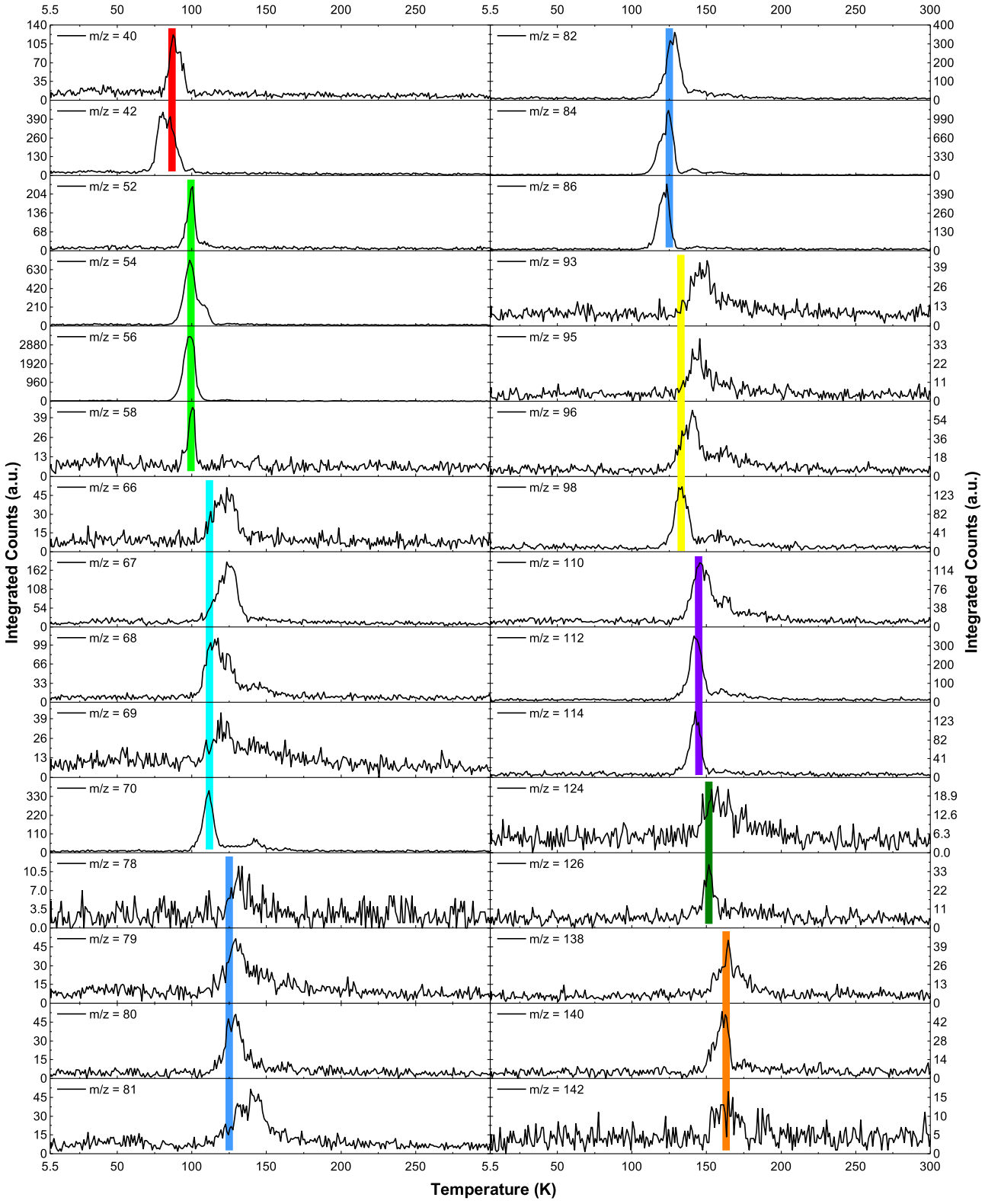

Figure 14. TPD profiles recorded via PI-ReTOF-MS corresponding to C3 (red), C4 (bright green), C5 (light blue), C6 (blue), C7 (yellow), C8 (purple), C9 (dark green), and C10 (orange), respectively, in the subliming ethane (C_2H_6) sample after irradiation.

(Figure 9). The detection of C_4H_4, C_5H_6, and C_6H_8 could be useful in determining the dosage needed to produce highly unsaturated hydrocarbon species. Vuitton et al. (2012) investigated the formation mechanism of hydrocarbons on Titan by proposing reactions incorporating the production of C_4H_4, including vinylacetylene ($H_2CCHCCH$; IE = 9.58 eV), from C_4H_2/C_4H_3, but suggesting that C_4H_4 isomers will also produce C_4H_2 species by photolysis.

4.6. Sublimation Temperatures

Next, we discuss the exploitation of the sublimation temperatures of the hydrocarbons to further verify our

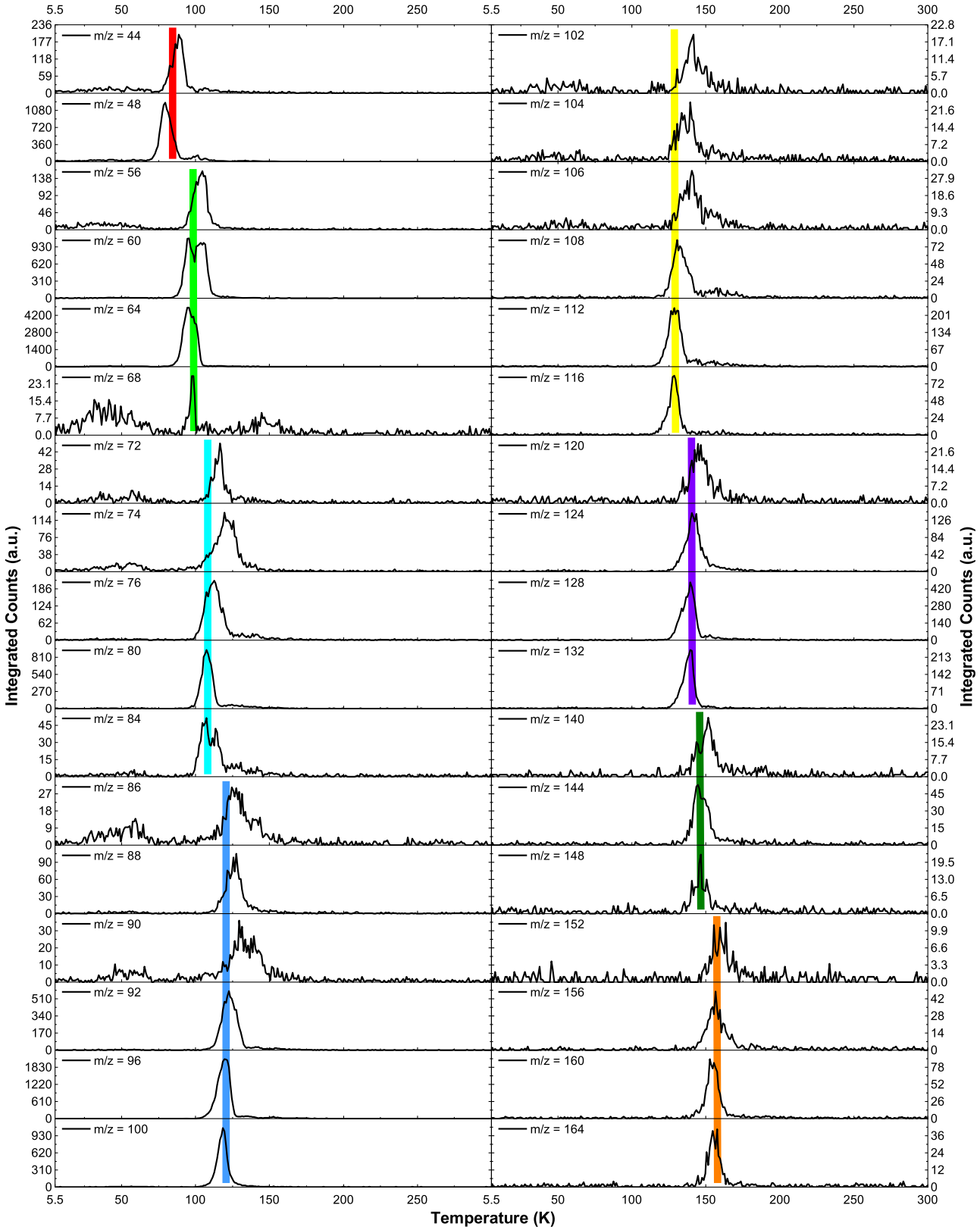

Figure 15. TPD profiles recorded via PI-ReTOF-MS corresponding to C3 (red), C4 (bright green), C5 (light blue), C6 (blue), C7 (yellow), C8 (purple), C9 (dark green), and C10 (orange), respectively, in the subliming D6-ethane (C_2D_6) sample after irradiation.

assignments. Figure 10 compiles the sublimation temperatures for the C_nH_{2n+2} (n = 4, 6, 8, 10), C_nH_{2n} (n = 3–10), C_nH_{2n-2} (n = 3–10), and C_nH_{2n-4} (n = 4–6) groups from the current study, as well as the sublimation data produced from methane irradiation experiments by Jones & Kaiser (2013). The sublimation temperatures depict an excellent agreement for

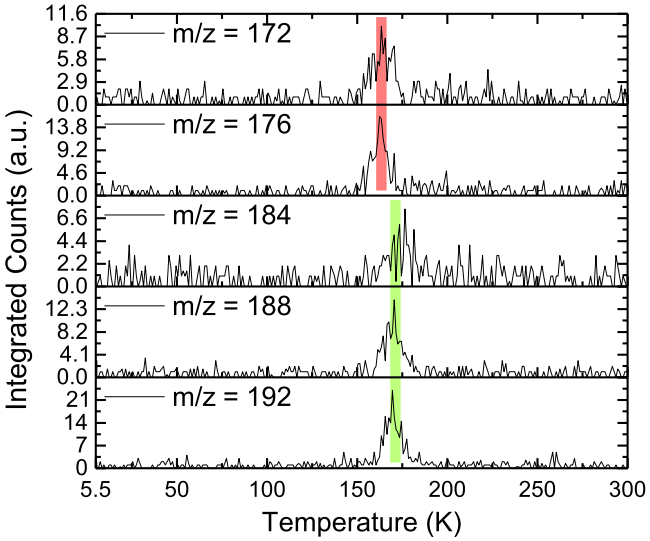

Figure 16. TPD profiles recorded via PI-ReTOF-MS corresponding to C11 (light red) and C12 (lime green) molecules in D6-ethane (C_2D_6) ices that were not observed in ethane (C_2H_6) ices.

the hydrocarbons that can be cross referenced between the methane and ethane experiments (Appendix A.5). Also, the sublimation temperature versus the mass-to-charge ratio observed does not show a linear trend, but rather a second-degree polynomial fit. The temperature increase for each additional carbon (or dicarbon) unit also allows the prediction of the temperature at which the next hydrocarbon will sublime; these data may be useful for determining in which regions of the ISM—depending on the temperature and ice—certain hydrocarbons carrying a dipole moment may be detectable.

In the current study, onset sublimation temperatures for alkanes were detected at $m/z = 58$ ($C_4H_{10}^+$, 93 K), $m/z = 86$ ($C_6H_{14}^+$, 111 K), $m/z = 114$ ($C_8H_{18}^+$, 129 K), and $m/z = 142$ ($C_{10}H_{22}^+$, 152 K). C_nH_{2n} sublimation onset temperatures were probed via $m/z = 42$ ($C_3H_6^+$, 72 K), $m/z = 56$ ($C_4H_8^+$, 88 K), $m/z = 70$ ($C_5H_{10}^+$, 100 K), $m/z = 84$ ($C_6H_{12}^+$, 111 K), $m/z = 98$ ($C_7H_{14}^+$, 121 K), $m/z = 112$ ($C_8H_{16}^+$, 131 K), $m/z = 126$ ($C_9H_{18}^+$, 140 K), and $m/z = 142$ ($C_{10}H_{20}^+$, 149 K). For C_nH_{2n-2}, sublimation onsets were detected at $m/z = 40$ ($C_3H_4^+$, 81 K), $m/z = 54$ ($C_4H_6^+$, 88), $m/z = 68$ ($C_5H_8^+$, 102 K), $m/z = 82$ ($C_6H_{10}^+$, 113 K), $m/z = 96$ ($C_7H_{12}^+$, 124 K),

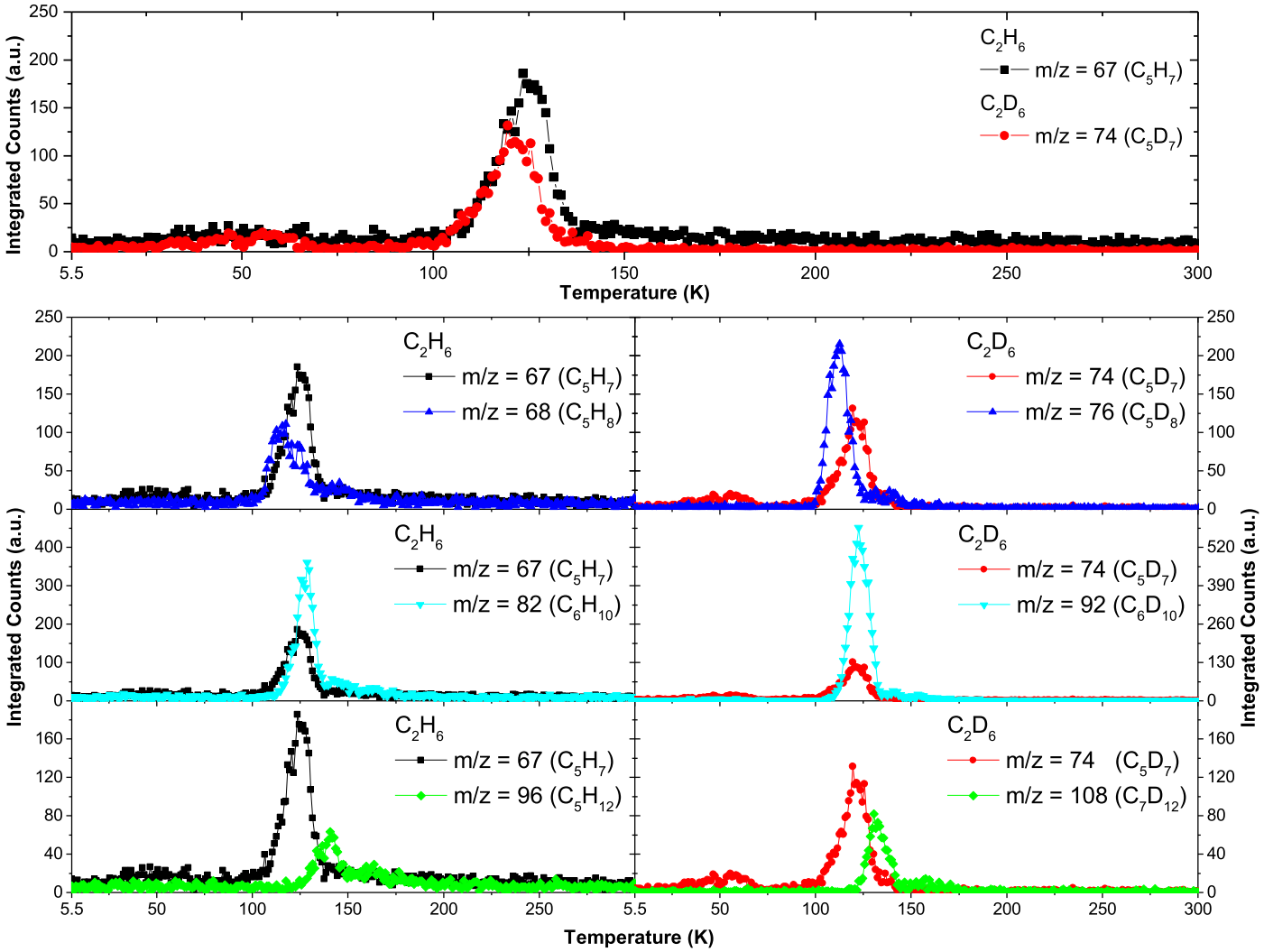

Figure 17. TPD profile of distinct ions corresponding to $C_5H_7^+/C_5D_7^+$, which are likely fragments from a C_6H_{10}/C_6D_{10} parent molecule. This is in agreement with appearance energies of this fragment; however, fragmentation of C_5H_8/C_5D_8 and C_7H_{12}/C_7D_{12} could also contribute slightly to the signal.

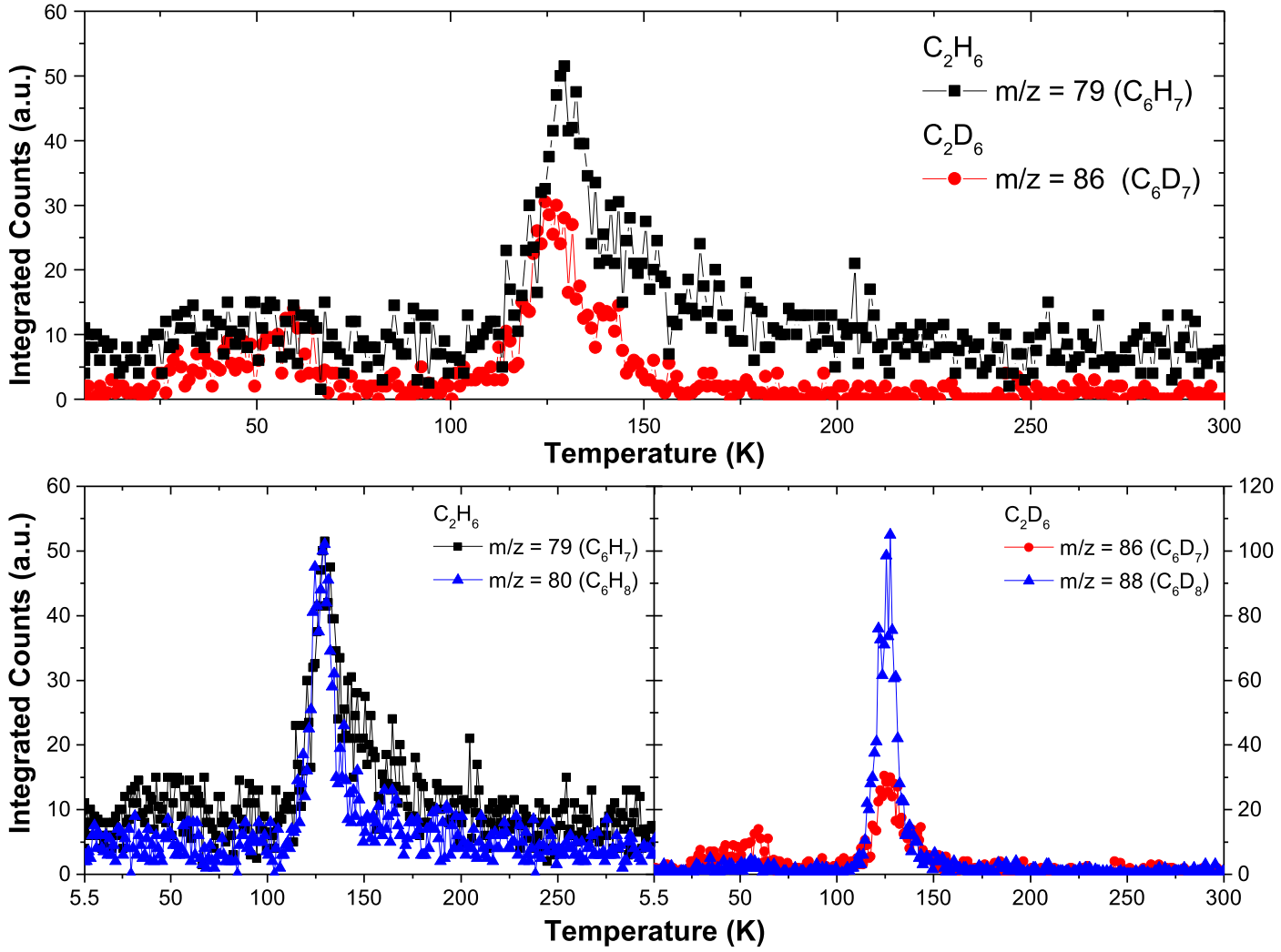

Figure 18. TPD profile of distinct ions corresponding to $C_6H_7^+/C_6D_7^+$, which are likely fragments from C_6H_8/C_6D_8 as the profiles are perfectly overlapping.

$m/z = 110$ ($C_8H_{14}^+$, 132 K), $m/z = 124$ ($C_9H_{16}^+$, 144 K), and $m/z = 138$ ($C_{10}H_{18}^+$, 150 K). Finally, the C_nH_{2n-4} temperatures of the sublimation onsets were detected at $m/z = 52$ ($C_4H_4^+$, 92), $m/z = 66$ ($C_5H_6^+$, 108 K), and $m/z = 80$ ($C_6H_8^+$, 116 K). These temperatures, as well as the complete sublimation profile, help to determine the validity of masses being possible fragments of a parent molecule (Appendix A.4).

4.7. Reaction Mechanism

Considering the infrared spectroscopic data and the detection of methane (CH_4), acetylene (C_2H_2), ethylene (C_2H_4), the ethyl radical (C_2H_5), 1-butene (C_4H_8), and *n*-butane (C_4H_{10}), along with kinetically fitting the coupled differential equation of the temporal concentration/column density profiles of the newly formed molecules, Kim et al. (2010) revealed that the radiation exposure of ethane by energetic electrons triggers a decomposition of a single ethane molecule (C_2H_6) via three competing pathways (reactions (1)–(3)) through the dominating molecular hydrogen (H_2) loss (reaction (1)), atomic hydrogen (H) ejection (reaction (2)), and carbene (CH_2) elimination (reaction (3)) as listed with decreasing branching ratios. With fractions of less than 1%, the ethyl radical (C_2H_5) can also decompose to ethylene (C_2H_4) (reaction (4)). If two ethane molecules are direct neighbors in the ice, the (formal) ethane dimer was found to eliminate molecular hydrogen and/or two hydrogen atoms leading to the one-step formation of *n*-butane (C_4H_{10}) (reaction (5)). However, the recombination of two ethyl radicals (C_2H_5) to *n*-butane (C_4H_{10}) (reaction (6)) represents the dominating pathway (99.99%) to *n*-butane (C_4H_{10}). The radiolysis of ethylene (C_2H_4) represents the prevailing route to acetylene (C_2H_2). The rate constants suggest that *n*-butane (C_4H_{10}) undergoes radiolysis very slowly with rate constants three orders of magnitude slower than the ethane (C_2H_6) to ethylene (C_2H_4) conversion to 1-butene (C_4H_8) (reaction (7)). With the exception of the radical–radical reactions, all pathways are highly endoergic since they require bond rupture processes and excess energy of between 0.4 and 4.8 eV. The latter can be supplied by the impinging electrons, which were determined to deposit 6.0 ± 1.1 eV in the C_2H_6 ice and processed (4.5 ± 1.2) × 10^{17} ethane molecules (Table 3).

$$C_2H_6\,(X^1A_{1g}) \rightarrow C_2H_4\,(X^1A_g) + H_2\,(X^1\Sigma_g^+) \quad (1)$$

$$C_2H_6\,(X^1A_{1g}) \rightarrow C_2H_5\,(XA') + H\,(^2S_{1/2}) \quad (2)$$

$$C_2H_6\,(X^1A_{1g}) \rightarrow CH_4\,(X^1A_1) + CH_2\,(a^1A_1) \quad (3)$$

$$C_2H_5\,(XA') \rightarrow C_2H_4\,(X^1A_g) + H(^2S_{1/2}) \quad (4)$$

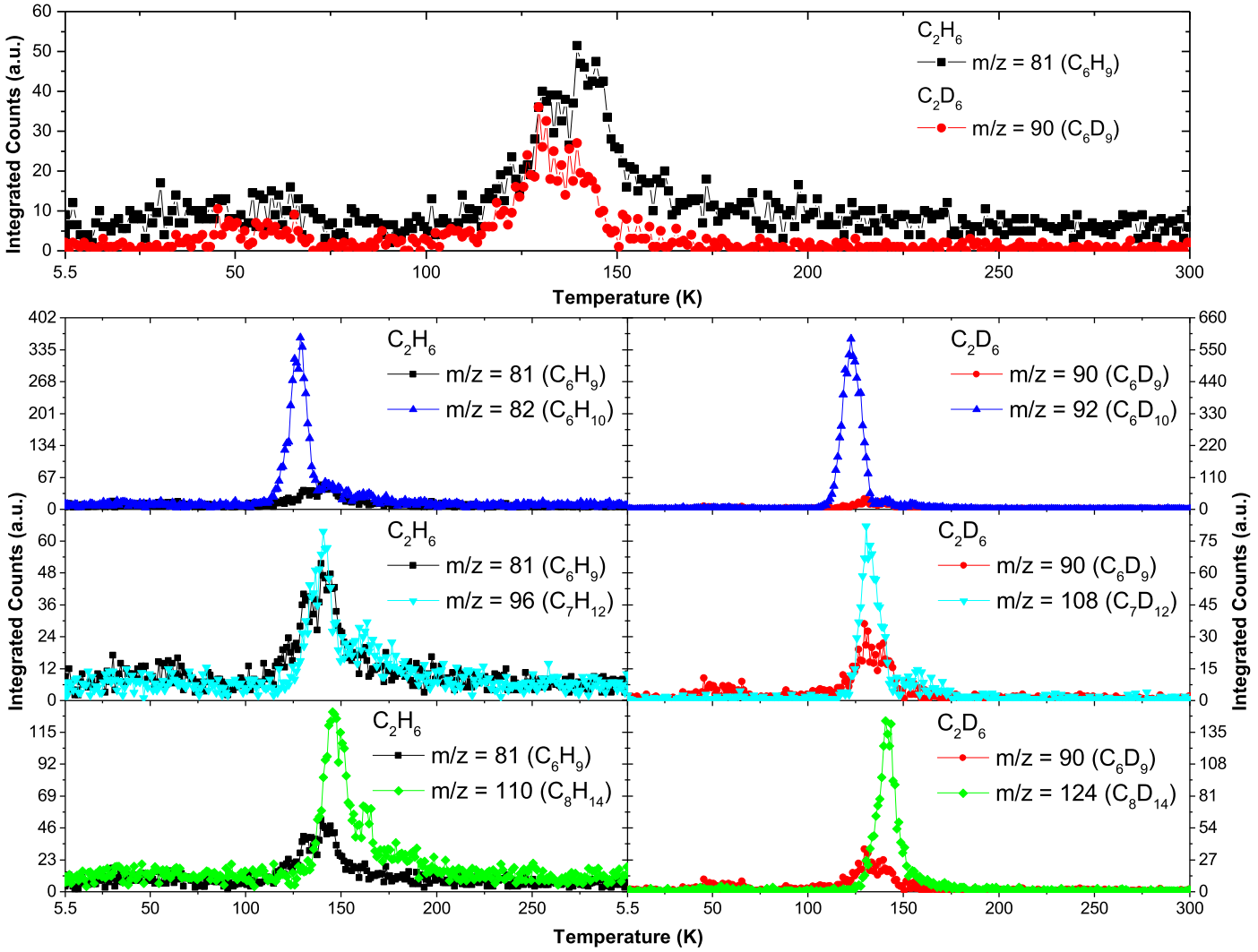

Figure 19. TPD profile of distinct ions corresponding to $C_6H_9^+/C_6D_9^+$, which are likely fragments from the C_7H_{12}/C_7D_{12} parent molecule. This is in agreement with appearance energies of this fragment; however, C_6H_{10}/C_6D_{10} and C_8H_{14}/C_8D_{14} could also contribute to the signal.

$$2\,C_2H_6\,(X^1A_{1g}) \rightarrow n\text{-}C_4H_{10}\,(X^1A_g) + H_2\,(X^1\Sigma_g^+)/2\,H(^2S_{1/2}) \quad (5)$$

$$2\,C_2H_5\,(XA') \rightarrow n\text{-}C_4H_{10}\,(X^1A_g) \quad (6)$$

$$n\text{-}C_4H_{10}\,(X^1A_g) \rightarrow 1\text{-}C_4H_8\,(X^1A) + H_2\,(X^1\Sigma_g^+). \quad (7)$$

Let us export these mechanisms and the aforementioned findings to rationalize the formation of more complex and highly unsaturated hydrocarbons. Considering the alkanes C_nH_{2n+2} (n = 3, 4, 6, 8, 10), various possible reaction pathways can be involved. Formally, carbene (CH_2) can be inserted into a carbon–hydrogen bond of an alkane, thus leading to a carbon chain growth by one carbon atom (reaction (8)); this mechanism represents the reversed reaction (3) in the case of methane. Alternatively, ethylene can be formally inserted into a carbon–hydrogen bond, thus resulting in a chain growth by two carbon atoms (reaction (9)). Further, the alkane can be first radiolyzed, losing a hydrogen atom (reaction (10)) requiring 21 kJ mol^{-1} (4.36 eV) (Irle & Morokuma 2000) in the case of the ethane–ethyl conversion. Then the alkyl radical can recombine unimpeded—if nearby—either with a methyl (CH_3) or ethyl radical (C_2H_5), thus growing the hydrocarbon chain by one and two carbon atoms, respectively (reactions (11) and (12)). Which represents the likely pathway? The formation of propane (C_3H_8)—the only odd carbon hydrocarbon—can only proceed via reaction of ethane or ethyl via carbene insertion or methyl recombination following schemes (8) and (11), respectively. Since the methyl radical was not detected, and only carbene has been inferred via its methane counter fragment (reaction (3)), the experiments suggest that propane is formed via reaction of ethane and carbene insertion (reaction (13)). Note that in related experiments of a nitromethane (CH_3NO_2) radiolysis, carbene (CH_2) was also identified as a crucial growth species leading from methyl nitrite (CH_3ONO) to ethyl nitrite (C_2H_5ONO) and from nitrosomethane (CH_3NO) to nitrosoethane (C_2H_5NO) (Kaiser & Maksyutenko 2015a, 2015b; Maksyutenko et al. 2015; Tsegaw et al. 2016; Turner et al. 2016). The even-numbered alkanes detected require C2 building blocks, i.e., ethylene and/or the ethyl radical. To date, no elementary reaction is known in which an ethylene molecule inserts into a carbon–hydrogen single bond, suggesting that reaction (9)—although formally feasible—does not produce any alkane. On the other hand, the recombination of two alkyl radicals via Equation (12) is well known to produce *n*-butane

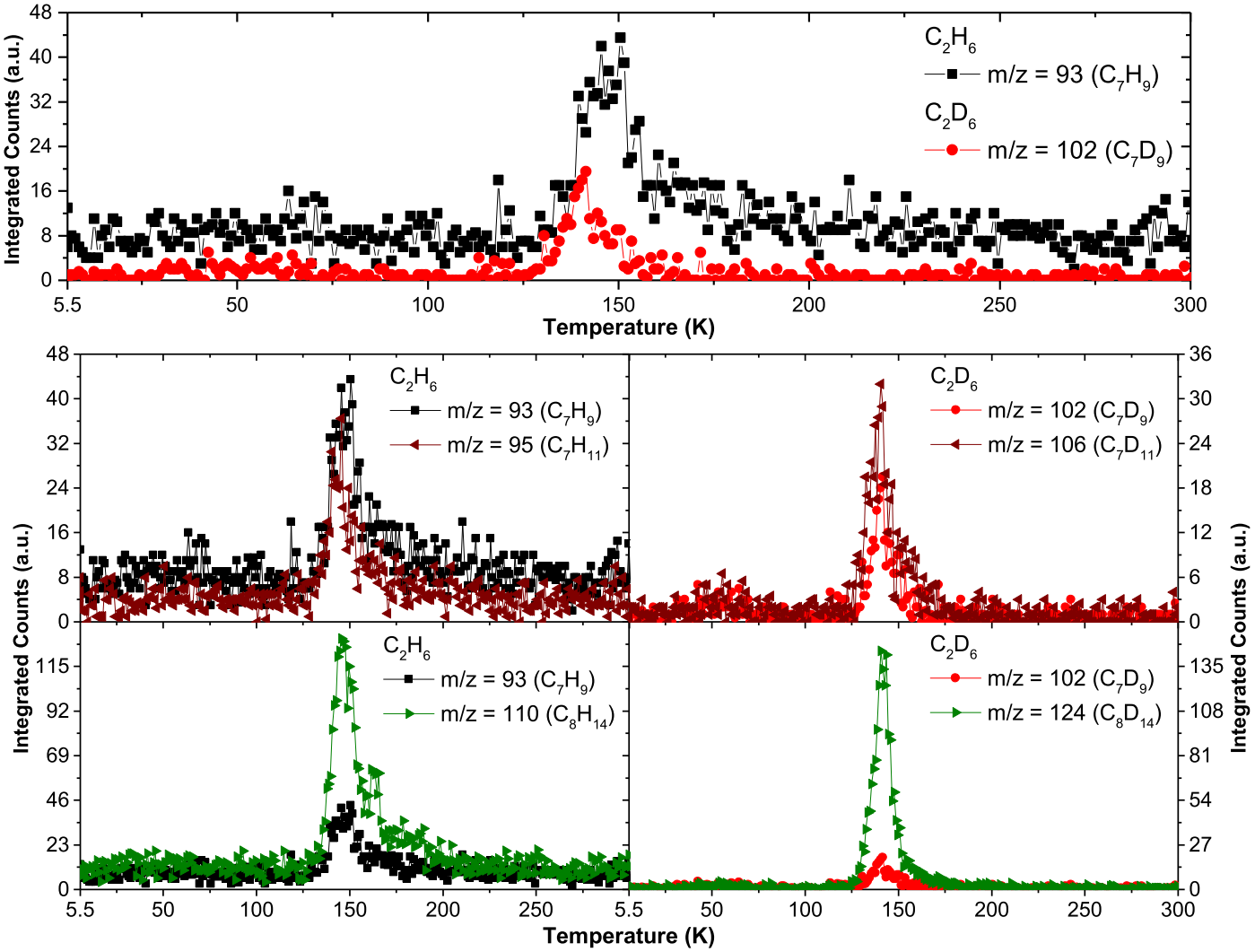

Figure 20. TPD profile of distinct ions corresponding to $C_7H_9^+/C_7D_9^+$, which are most likely fragments from C_8H_{14}/C_8D_{14} as the profiles depict a nearly perfect overlap.

(C_4H_{10}), which is easily accessible via reaction (6) as also found in this ethane experiment. Likewise, *n*-butane can be radiolyzed and ejects atomic hydrogen from the C1/C4 and/or C2/C3 site leading to *n*-butyl or *i*-butyl radicals; the latter can recombine with an ethyl radical, forming hexanes (C_6H_{14}), and this mechanism can expand up to decanes ($C_{10}H_{22}$) as detected in the present study.

Although the specific isomers of the alkanes (C_6H_{14}, C_8H_{18}, $C_{10}H_{22}$) are unknown, an assumption that they are all straight-chain (*n*-alkanes) type allows a determination of their relative abundances. Here, the signal for each ion was integrated from its sublimation onset temperature until the signal returned to the baseline; this raw signal was corrected using the photoionization cross sections at 10.5 eV for *n*-hexane (2.4 Mb), *n*-octane (3.1 Mb), and *n*-decane (3.7 Mb) (Adam & Zimmermann 2007). Using these photoionization cross sections, each signal was scaled, resulting in a ratio of 100 ± 4:26 ± 2:5 ± 1 (*n*-hexane:*n*-octane:*n*-decane) and 104 ± 3:35 ± 2:5 ± 1 for the deuterated sample. These data show an excellent agreement between the isotopologue relative abundances for these assumed *n*-alkanes. This approximation reinforces the proposed reaction mechanism that the larger alkanes are produced from a previous alkane via radiolysis and hydrogen atom loss (reaction (10)).

$$C_nH_{2n+2} + CH_2 \rightarrow C_{n+1}H_{2n+4} \quad (8)$$

$$C_nH_{2n+2} + C_2H_4 \rightarrow C_{n+2}H_{2n+6} \quad (9)$$

$$C_nH_{2n+2} \rightarrow C_nH_{2n+1} + H \quad (10)$$

$$C_nH_{2n+1} + CH_3 \rightarrow C_{n+1}H_{2n+4} \quad (11)$$

$$C_nH_{2n+1} + C_2H_5 \rightarrow C_{n+2}H_{2n+6} \quad (12)$$

$$C_2H_6 + CH_2 \rightarrow C_3H_8. \quad (13)$$

The even-numbered unsaturated hydrocarbons (C_nH_{2n})—along with propene (C_3H_6)—could be formed via dehydrogenation of the corresponding alkane precursors in a similar manner to how 1-butene (C_4H_8) results from molecular hydrogen loss from *n*-butane (C_4H_{10}) (Equation (7)). This also gains support since the highest members of both alkanes and alkenes with 10 carbon atoms have been observed. The propene molecule (C_3H_6) might act as a building block for up to three sequential hydrogen atom losses—versus ethyl (C_2H_5) replacement via ethyl addition—with the hydrogen atom elimination at the carbon–carbon double bond of propylene yielding eventually C_9H_{18}. It should be noted that cyclopropane (C_3H_6) could also be formed—here via addition of

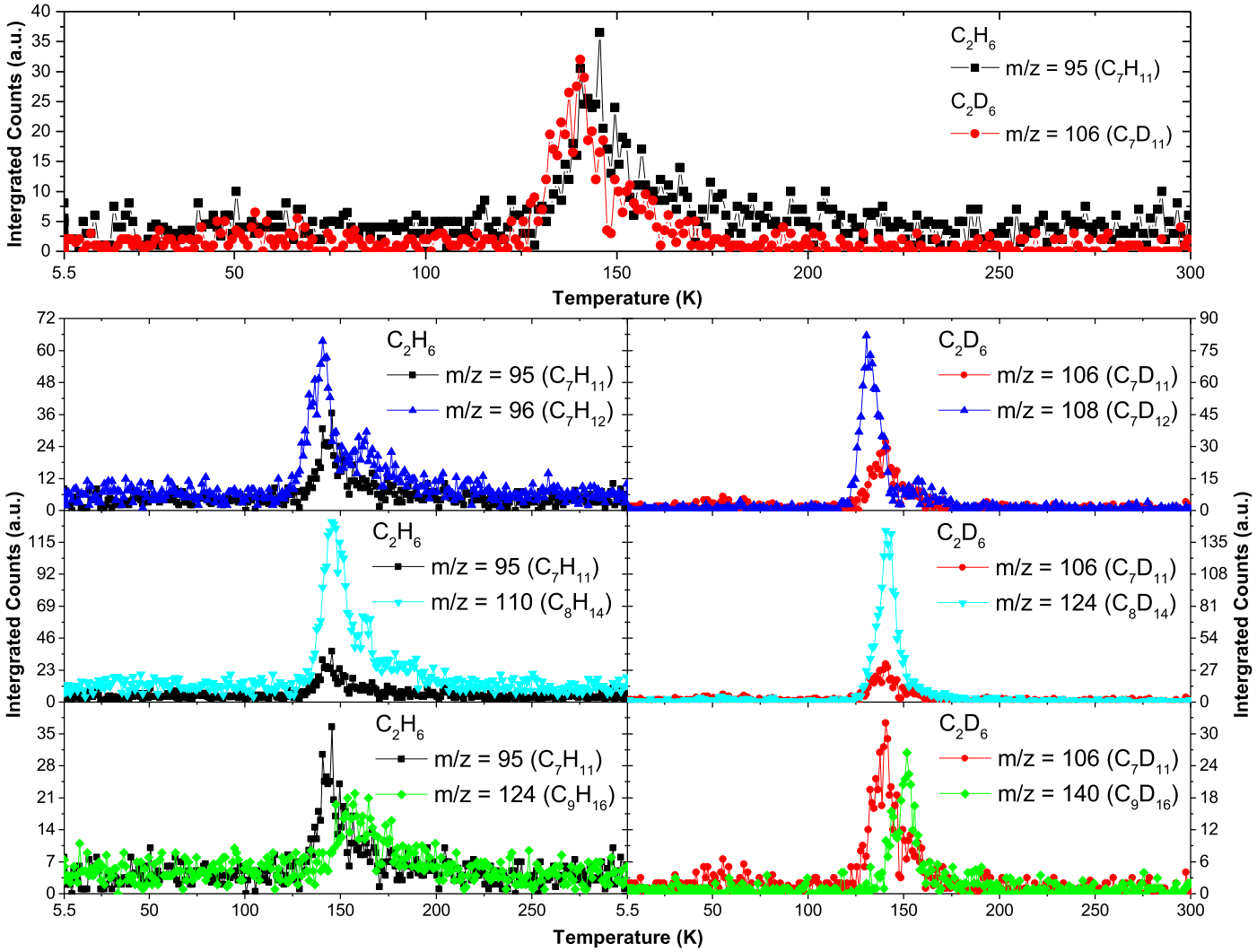

Figure 21. TPD profile of distinct ions corresponding to $C_7H_{11}^+/C_7D_{11}^+$, which are likely fragments from a C_7H_{12}/C_7D_{12}parent molecule. This is in agreement with appearance energies of this fragment; however, fragmentation from C_8H_{14}/C_8D_{14} and C_9H_{16}/C_9D_{16} could also contribute to the signal.

carbene to the carbon–carbon double bond of ethylene. Recall that formally C_nH_{2n} could also represent cycloalkanes. Finally, the hydrogen deficient species C_nH_{2n-2} (n = 3–10) and C_nH_{2n-4} (n = 4–6) could be synthesized via step-wise dehydrogenation from their saturated counterparts. Detailed mechanisms cannot be extracted at the present stage.

5. ASTROPHYSICAL IMPLICATIONS

Although pure ethane ices have not been detected in either the ISM or our solar system, small hydrocarbons (C1 and C2) have been observed in both environments. Methane and ethane have been probed on Titan (Griffith et al. 2006), Pluto (Holler et al. 2014), Makemake (Brown et al. 2015), and Quaoar (Dalle Ore et al. 2009). Also, low-temperature interstellar ices have been shown to primarily contain water (H_2O), ammonia (NH_3), carbon dioxide (CO_2), carbon monoxide (CO), methanol (CH_3OH), and even methane (CH_4), with the latter at a level of a few percent (Boogert et al. 2015). The processing of methane ices has shown the facile production of the C2 hydrocarbons ethane, ethylene, and acetylene (Bennett et al. 2006); the exposure of ethane ices to ionizing radiation depicts the production of methane, ethylene, and acetylene (Kim et al. 2010). These C1 and C2 hydrocarbons are building blocks of aromatic systems from benzene (Zhou et al. 2010) up to polycyclic aromatic hydrocarbons (PAHs) (Kaiser & Roessler 1997; Jones & Kaiser 2013). Therefore, an understanding of the chemistry of the C1 and C2 hydrocarbon species is crucial for a complete understanding of the formation of hydrocarbons in interstellar and planetary ices.

More specifically, the present experiment revealed six individual molecules via their infrared signatures: methane [CH_4 (CD_4)], acetylene [C_2H_2 (C_2D_2)], ethylene [C_2H_4 (C_2D_4)], the ethyl radical [C_2H_5 (C_2D_5)], 1-butene [C_4H_8 (C_4D_8)], and n-butane [C_4H_{10} (C_4D_{10})]. These identifications are in line with previous experiments (Scheer et al. 1962; Jackson et al. 1966; Hudson et al. 2009; Kim et al. 2010) and agree that the production of C1 to C4 hydrocarbons is feasible in processed ethane ices. However, once the processed ethane ices were warmed up, which simulates the transition of a molecular cloud to a star-forming region or comets approaching the Sun, four groups of hitherto elusive hydrocarbons were detected: C_nH_{2n+2} (n = 4, 6, 8, 10), C_nH_{2n} (n = 3–10), C_nH_{2n-2} (n = 3–10), and C_nH_{2n-4} (n = 4–6). The identification of this variety of hydrocarbons suggests that

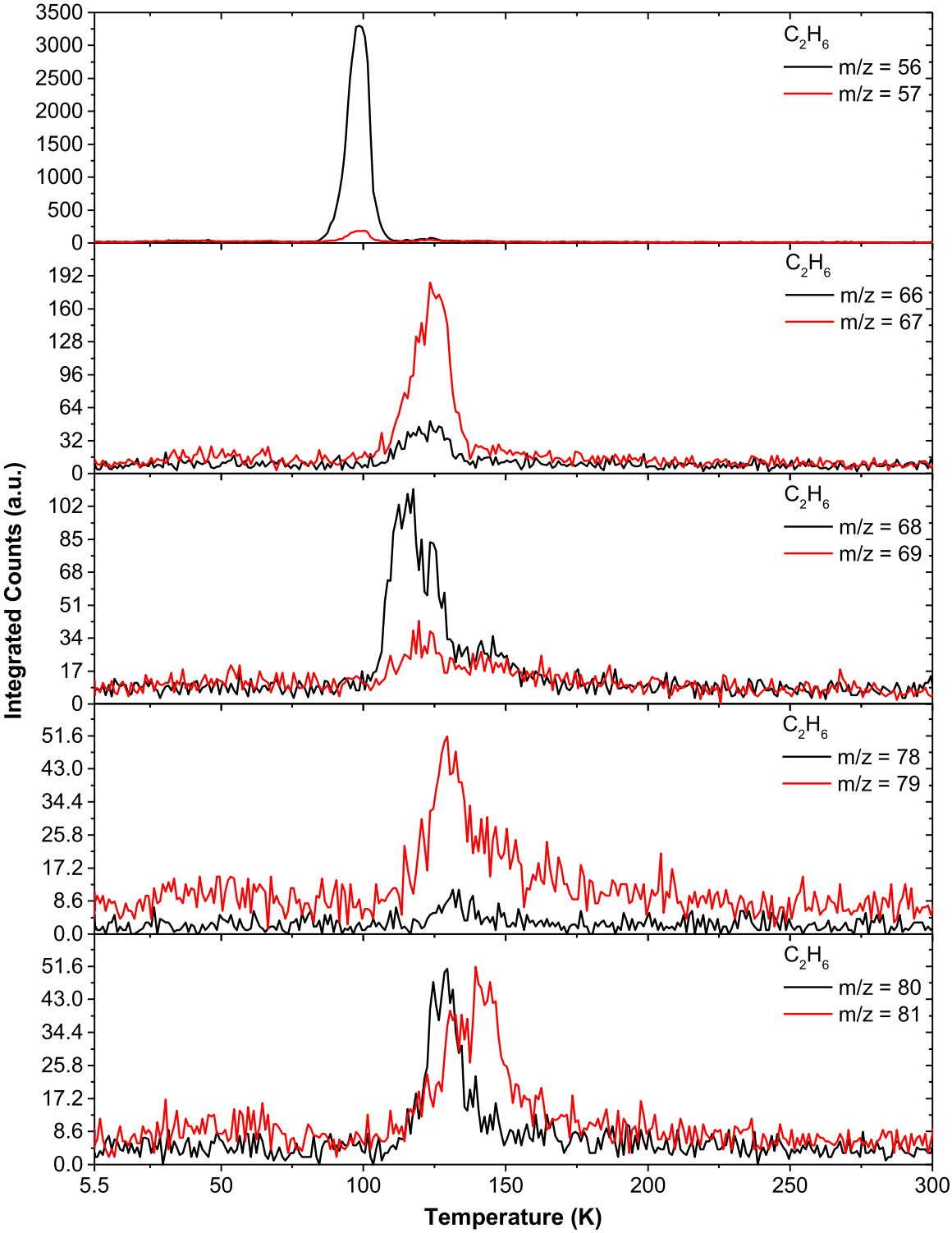

Figure 22. Overlay of sublimation profiles of products from ethane (C_2H_6) ices with prospective ^{13}C isotopologues.

complex hydrocarbon chemistry takes place in the processed hydrocarbon ices. These species hold crucial astrophysical implications.

From the C_nH_{2n} hydrocarbon group, the propylene molecule (CH_2CHCH_3) has been repeatedly shown to contribute in the formation of resonantly stabilized free radicals (RSFRs)—precursors to PAHs—in gas phase reactions. Crossed molecular beams experiments of the reaction of propylene (CH_2CHCH_3; X^1A') with carbon atoms (C; ^3P_j) (Kaiser et al. 1997b) and dicarbon molecules (C_2; $X^1\Sigma_g^+/a^3\Pi_u$) (Dangi et al. 2013) revealed the formation of the methylpropargyl radical (C_4H_5) as well as 1- and 3-vinylpropargyl, respectively. The interactions with carbon atoms and dicarbon molecules produced the necessary precursors for PAH formation, while reactive collisions with the cyano radicals (CN) resulted in the production of organic nitriles such as 1- and 3-cyanopropylene.

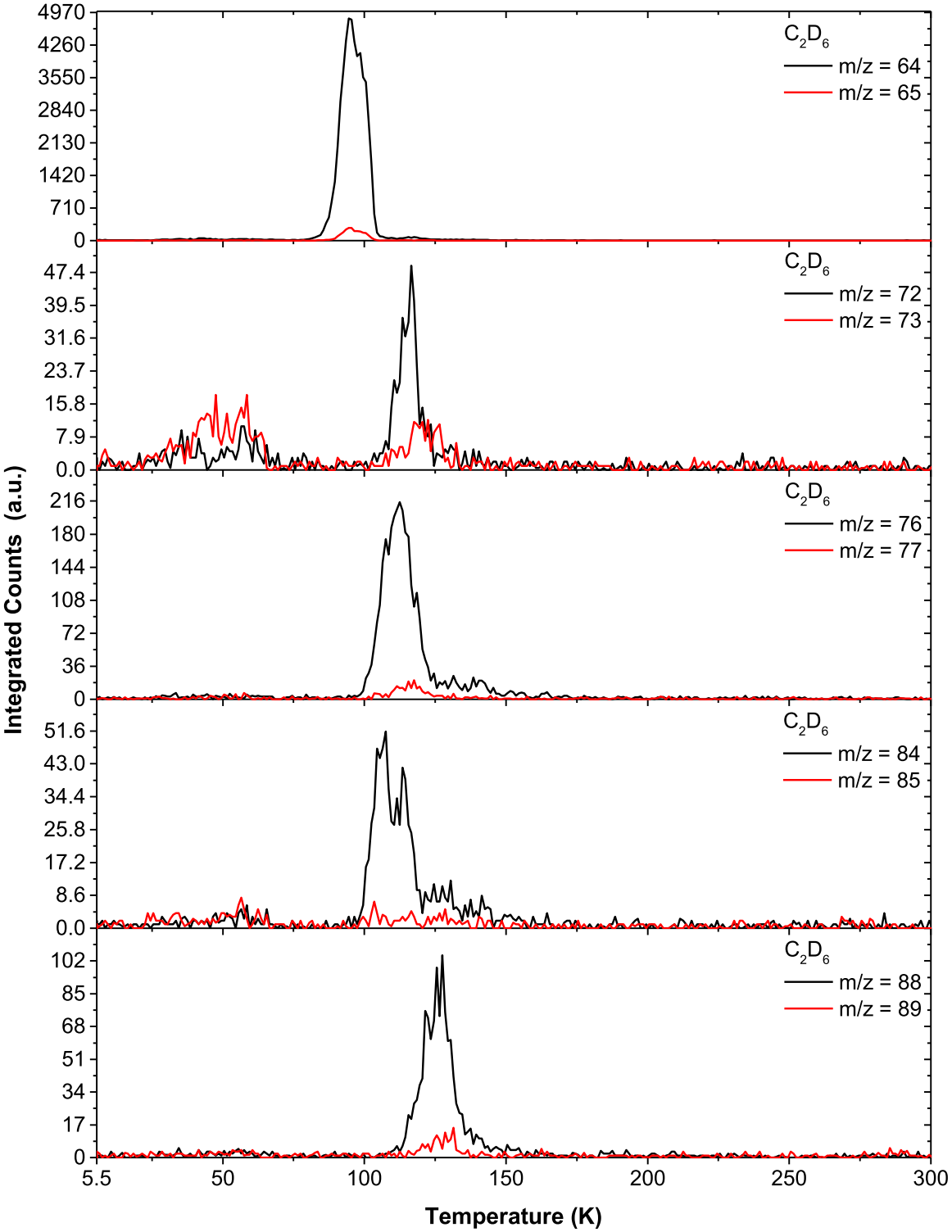

Figure 23. Overlay of sublimation profiles of products from D6-ethane (C_2D_6) ices with prospective ^{13}C isotopologues.

Further, the C_3H_4 isomers methylacetylene (CH_3CCH) and allene (H_2CCCH_2) represent two astrophysically important molecules that belong to the C_nH_{2n-2} group. Besides playing roles in Titan's atmospheric chemistry (Vakhtin et al. 2001; Goulay et al. 2007; Zhang et al. 2009) these isomers have been proven to be very important in interstellar chemistry. Specifically, both isomers are proposed to assist in the formation of PAHs (Yang et al. 2015) and in particular of indene (C_9H_8) in the reaction with the phenyl radical (C_6H_5) (Zhang et al. 2011; Parker et al. 2015, 2011). Another astrochemically relevant molecule from this hydrocarbon group is the C_4H_6 isomer 1, 3-butadiene ($H_2CCHCHCH_2$). The gas phase reaction of 1, 3-butadiene with the ethynyl radical (CCH) produces benzene (C_6H_6) in the ISM (Jones et al. 2011).

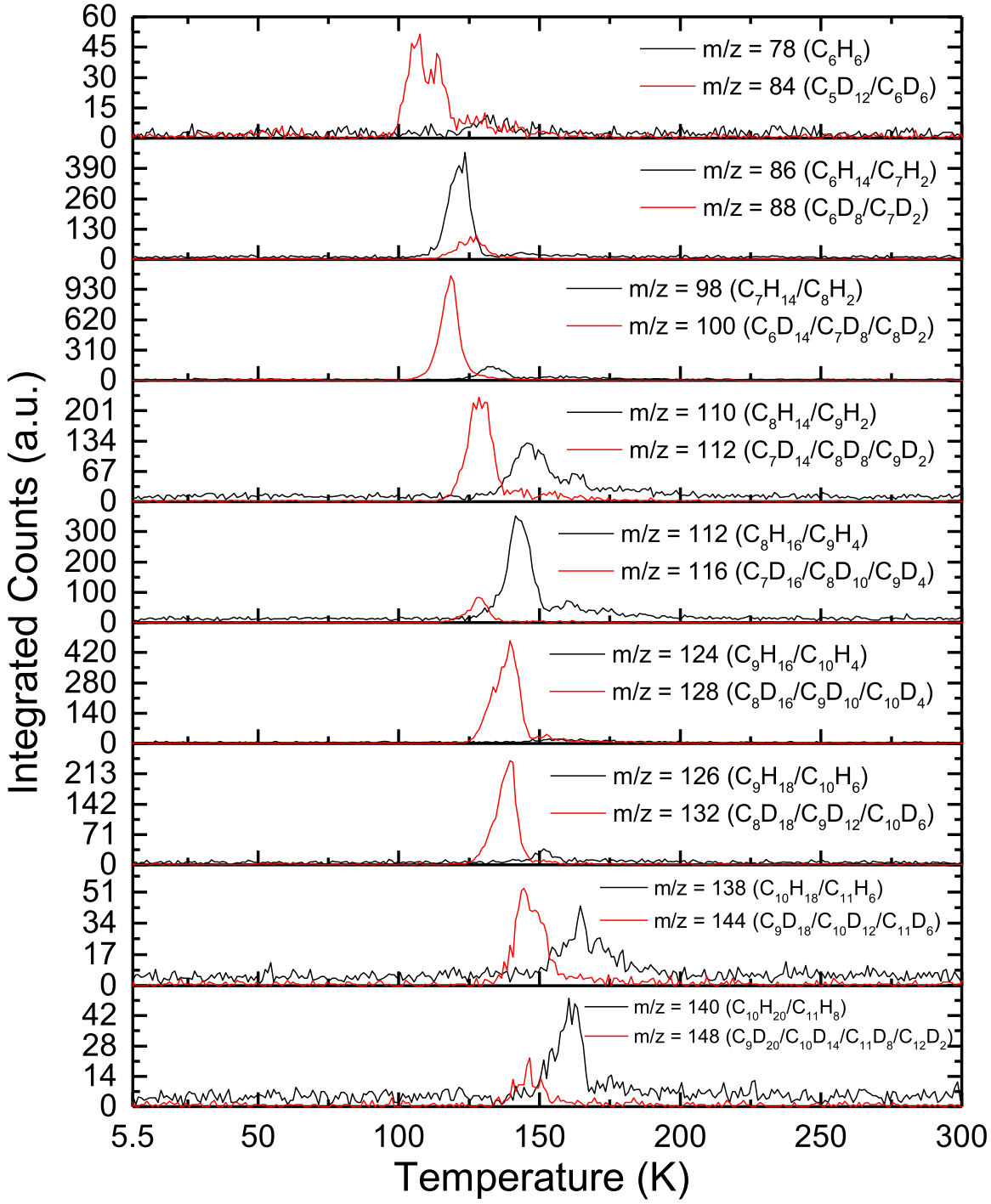

Figure 24. Overlay of distinct mass-to-charge ratios with multiple molecular formulae observed in the ethane (C_2H_6) experiments with the corresponding mass-to-charge ratios of these alternate molecular formulae detected in the D6-ethane (C_2D_6) experiments in order to compare TPD profiles and determine if there are multiple possible contributors to these signals.

Also, the C_nH_{2n-4} group has some important molecules including the C_4H_4 isomer vinylacetylene ($H_2CCHCCH$). Here, the reaction of vinylacetylene ($H_2CCHCCH$) with the phenyl radical (C_6H_5) produces the prototype PAH molecule, naphthalene ($C_{10}H_8$), even at 10 K in the gas phase (Parker et al. 2012).

As previously stated, ethane has been detected on several solar system bodies and is the major photochemical product in Titan's atmosphere (Coustenis et al. 1999). Coustenis et al. (1999) stated that several hydrocarbons—detected in the present study by the processing of solid ethane—could be present on Titan and help explain observed spectroscopic features. However, a methane-dominated lake, Ligeia Mare, was detected on Titan and the possible sequestration of ethane in clathrates may be possible (Mousis & Schmitt 2008; Mousis et al. 2016). Hunten (2006) suggested that the missing amounts of ethane and propane (Nixon et al. 2009) on Titan is due to sequestration in the "dust" or "sand" dunes observed on Titan. Toftmann et al. (2005) modeled the effect of cosmic rays on Titan and revealed that they are capable of penetrating deep

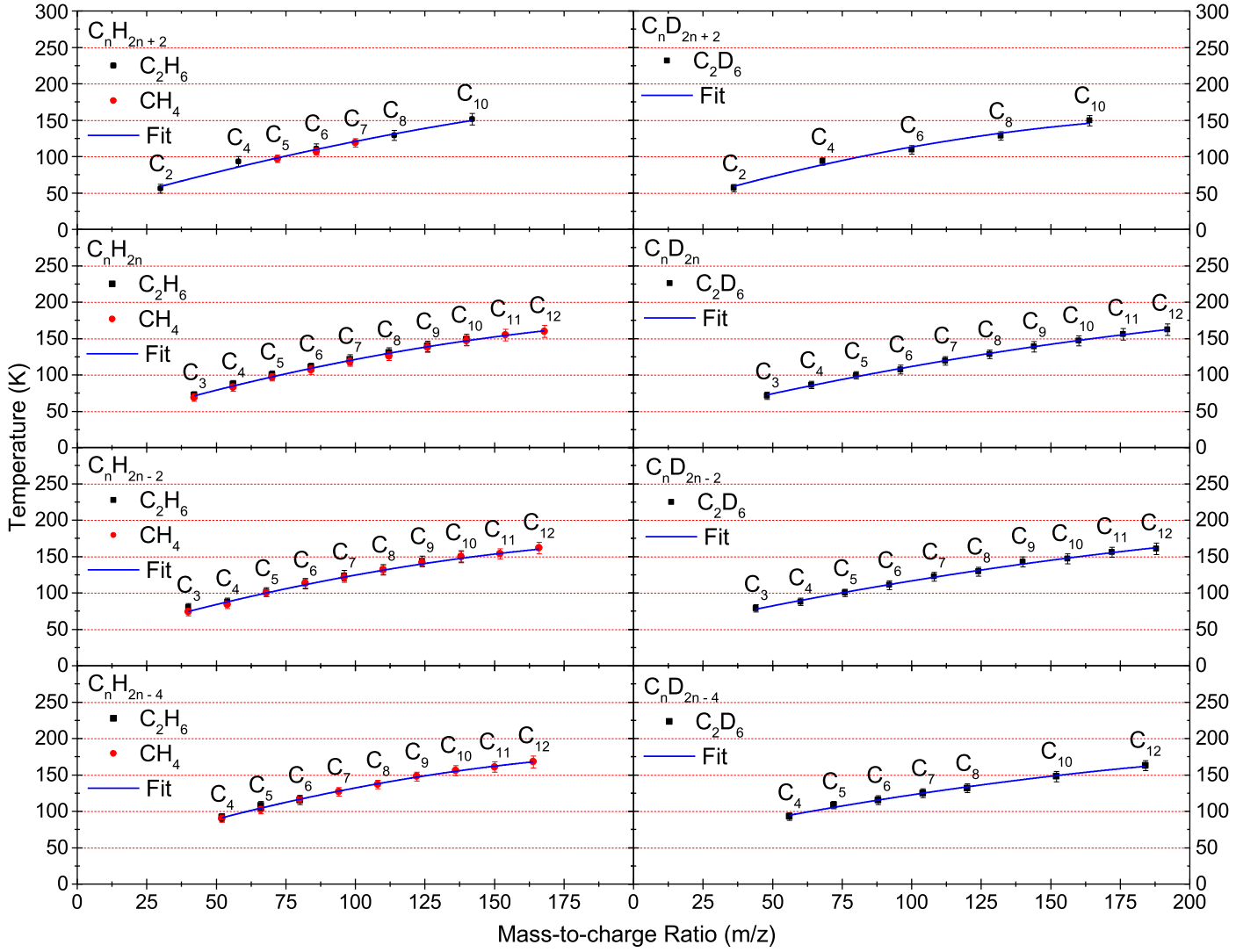

Figure 25. Sublimation onset temperatures of C_nH_{2n+2} (n = 4, 6, 8, 10) (left), C_nH_{2n} (n = 3–10), C_nH_{2n-2} (n = 3–10), C_nH_{2n-4} (n = 4–6), (right) C_nD_{2n+2} (n = 4, 6, 8, 10), C_nD_{2n} (n = 3–12), C_nD_{2n-2} (n = 3–12), and C_nD_{2n-4} (n = 4–12). Black points are from irradiated ethane (C_2H_6; left) and D6-ethane (C_2D_6; right), and red ones are from irradiated methane (CH_4) ices from Jones & Kaiser (2013).

into the lower atmosphere, which allows them to interact with the newly formed ethane and possibly promote the chemistry that has been shown in the present experiment. The penetration of GCRs into Titan's atmosphere also can lead to the incorporation of oxygen into hydrocarbons and possibly produce prebiotic chemicals (Sittler et al. 2009). Pluto is also processed with both the solar wind (Cravens & Strobel 2015) and Lyα photons (Gladstone et al. 2015), and an expected radiation dose for trans-Neptunian objects (TNOs) was calculated to be about 22 eV for each ethane molecule (Hudson et al. 2009). Our experiments showed chemical complexity in the ethane ice when only a 7 eV dose was applied and suggests that TNOs with ethane ice may hold a very complex array of hydrocarbons among other COMs. Also, alkanes were suggested to contribute to certain features in Pluto's spectra by studying several linear and branched alkanes diluted in nitrogen ice (Bohn et al. 1994). Recently, Lorenzi et al. (2016) suggested that the discoloration of Pluto along with Makemake and Eris may be due to COMs, and our present study shows that this is very likely just from the simple ethane ice. Dangi et al. (2015) has shown that under model atmospheric conditions containing C3 and C4, hydrocarbons interact catalytically with surfaces of micrometeroids to produce a carbonaceous refractory layer, which can account for the hydrocarbon sequestration.

Although laboratory astrochemistry experiments have been carried out for many years, the data that are gathered by the help of emerging experimental techniques such PI-ReTOF-MS continues to evolve and provide further evidence that there is a very complex chemistry taking place within interstellar ices. Therefore, a systematic study of simple analog ices is needed to further develop the understanding of formation pathways present in these ices before attempting to investigate complex model interstellar ices. In the current experiment the processing of a pure ethane ice has shown that a complex assortment of molecules, many which have been detected for the first time, with the generic formulas of C_nH_{2n+2}, C_nH_{2n}, C_nH_{2n-2}, and C_nH_{2n-4}, were able to be formed via processing with energetic electrons representing secondary electrons generated via GCRs. This ice may be viewed as model ice, but without a systematic understanding of the chemical complexity possible within each ice constituent of a more complex model ice, our understanding will be lacking important mechanistic details. This study

represents a bottom-up approach to investigating the extra-terrestrial hydrocarbon chemistry that can also be applied to the chemical pathways present in our solar system on different objects. Future experiments are being designed to elucidate which specific C3 and C4 hydrocarbon isomers are being produced via *tunable* PI-ReTOF-MS from this simple ethane ice. The results from these studies will further elucidate the formation mechanisms taking place within the processed ethane ice and will help to constrain the chemical complexity capable of being initiated in this simple system. As discussed above there are several possible C3 and C4 isomers that have been proven to have large astrophysical implications and the untangling of their production or non-production from the ethane ice can lead to a further understanding of the chemical pathways needed to produce complex molecules in astrophysical environments.

R.I.K. and M.J.A. thank the US National Science Foundation (AST-1505502) for support conducting the experiments and data analysis. We thank Dr. Brant Jones (Newport) for experimental assistance. The setup was financed by the W. M. Keck Foundation through an equipment grant.

APPENDIX

A.1. Infrared Spectroscopy-C_2D_6

The FTIR in situ analysis was carried out for the D6-ethane (C_2D_6) ice during the irradiation and new infrared absorptions were detected confirming the assignments of the ethane (C_2H_6) ice. Fundamentals corresponding to methane (CD_4), acetylene (C_2D_2), ethylene (C_2D_4), the ethyl radical (C_2D_5), 1-butene (C_4D_8), and *n*-butane (C_4D_{10}) were assigned (Table 1(b), Figure 11).

A.2. Mass Spectrometry—RGA Results

The RGA detected signals for several important mass-to-charge ratios during the TPD. These could be attributed to the ethane (C_2H_6/C_2D_6, reactant; $m/z = 30/36$), propane (C_3H_8/C_3D_8, product; $m/z = 44/52$), and butane (C_4H_{10}/C_4D_{10}, product; $m/z = 58/68$) via their molecular ions (Figure 12). The ethane reactant was observed to start subliming at about 57 K with a maximum at 70 K. Meanwhile, the propane sublimation profile had an onset temperature of 75 K and depicts a bi-modal structure with maxima at 81 and 100 K. The bi-modal shape is likely due to a fraction of this product being trapped within the newly formed butane products considering the identical sublimation profiles of the second propane peak and of the butane profile. However, as previously discussed, the use of an electron impact ionizer at 100 eV will result in a major reduction in signal of the molecular ion for larger hydrocarbons identified here. Therefore, we turn to the more sensitive mass spectrometry technique PI-ReTOF-MS.

A.3. Mass Spectrometry—PI-ReTOF-MS

The analyses of the subliming molecules from the irradiated D6-ethane ice via PI-ReTOF-MS utilizing 10.49 eV photons are summarized in Figure 13 and Table 2. Figure 13 shows the intensity of mass-to-charge ratio signals as a function of temperature for the irradiated ethane (C_2D_6) ices with detected mass-to-charge ratios close to $m/z = 200$.

A.4. Mass Spectrometry—Other Masses

Seven ions detected in the gas phase analysis did not correspond to the groups as discussed in 4.2–4.5. These ions carry all odd mass-to-charge ratios of $m/z = 57$, $m/z = 67$, $m/z = 69$, $m/z = 79$, $m/z = 81$, $m/z = 93$, and $m/z = 95$. First, a complete comparison of all ion sublimation profiles was analyzed and the sublimation onset of each carbon group was shaded and extended to all other ions in the same group to determine if they could be fragments from the largest hydrocarbon in that group (Figures 14–16). The suspect molecules were then investigated further. These odd mass ions may be mainly described by the natural isotopic abundance of ^{13}C in the sample, and the comparison of these signal intensities to the ^{12}C isotopologues can determine if this is the correct answer. The alternate explanation of the odd ions is that they are a product of the molecular ion fragmenting. A large number of hydrocarbons are not able to fragment at a photoionization energy of 10.49 eV, however, larger and more exotic hydrocarbons are much more readily fragmented even at 10.49 eV (Lias et al. 2016). The following ions were assigned as $m/z = 57$ ($^{13}CC_3H_8^+$) and $m/z = 69$ ($^{13}CC_4H_8^+$), as each displayed the expected signal intensities for natural isotopic substitution of ^{13}C (Figures 14–24). Meanwhile $m/z = 67$ ($C_5H_7^+$), $m/z = 79$ ($C_6H_7^+$), $m/z = 81$ ($C_6H_9^+$), $m/z = 93$ ($C_7H_9^+$), and $m/z = 95$ ($C_7H_{11}^+$) were associated with fragments (Figures 17–21). Each of these ions was analyzed under both conditions to understand how each of these odd ions is produced. It is important to reiterate that since both C_2H_6 and C_2D_6 ices were analyzed each questionable fragment or isotope was cross-analyzed between systems (Figure 24). This technique has been shown to be a useful tool in determining mass-to-charge ratios that do not directly correspond to an expected molecular ion (Turner et al. 2015, 2016).

A.5. Sublimation Temperatures—C_2D_6

Next, we discuss the exploitation of sublimation temperature of the hydrocarbons to further verify our assignments. Figure 25 compiles the sublimation temperatures for the C_nH_{2n+2} ($n = 4$, 6, 8, 10), C_nH_{2n} ($n = 3$–10), C_nH_{2n-2} ($n = 3$–10), C_nH_{2n-4} ($n = 4$–6), C_nD_{2n+2} ($n = 4$, 6, 8, 10), C_nD_{2n} ($n = 3$–12), C_nD_{2n-2} ($n = 3$–12), and C_nD_{2n-4} ($n = 4$–12) groups from the current study, as well as the sublimation data produced from methane irradiation experiments by Jones & Kaiser (2013). The sublimation temperatures depict an excellent agreement for the hydrocarbons that can be cross referenced between all three experiments: CH_4, C_2H_6, and C_2D_6.

REFERENCES

Abou Mrad, N., Duvernay, F., Theulé, P., Chiavassa, T., & Danger, G. 2014, AnaCh, 86, 8391
Abplanalp, M. J., Borsuk, A., Jones, B. M., & Kaiser, R. I. 2015, ApJ, 814, 45
Abplanalp, M. J., Förstel, M., & Kaiser, R. I. 2016, CPL, 644, 79
Adam, T., & Zimmermann, R. 2007, Anal. Bioanal. Chem., 389, 1941
Belloche, A., Müller, H. S., Menten, K. M., Schilke, P., & Comito, C. 2013, A&A, 559, 1
Bennett, C. J., Jamieson, C. S., Osamura, Y., & Kaiser, R. I. 2005a, ApJ, 624, 1097
Bennett, C. J., Jamieson, C. S., Osumura, Y., & Kaiser, R. I. 2006, ApJ, 653, 792
Bennett, C. J., & Kaiser, R. I. 2007, ApJ, 660, 1289
Bennett, C. J., Osamura, Y., Lebar, M. D., & Kaiser, R. I. 2005b, ApJ, 634, 698
Bieri, G., Burger, F., Heilbronner, E., & Maier, J. P. 1977, Helvetica Chimica Acta, 60, 2213

Bohn, R. B., Sandford, S. A., Allamandola, L. J., & Cruikshank, D. P. 1994, Icar, 111, 151
Boogert, A. C. A., Gerakines, P. A., & Whittet, D. C. B. 2015, ARA&A, 53, 541
Brown, M. E., Schaller, E. L., & Blake, G. A. 2015, AJ, 149, 105
Callahan, M. P., Gerakines, P. A., Martin, M. G., Peeters, Z., & Hudson, R. L. 2013, Icar, 226, 1201
Caro, G. M. M., & Schutte, W. A. 2003, A&A, 412, 121
Charnley, S. B., Ehrenfreund, P., & Kuan, Y. J. 2001, AcSpA, 57, 685
Compagnini, G., D'Urso, L., Puglisi, O., Baratta, G. A., & Strazzulla, G. 2009, Carbon, 47, 1605
Costagliola, F., Sakamoto, K., Muller, S., et al. 2015, A&A, 582, A91
Coustenis, A., Schmitt, B., Khanna, R. K., & Trotta, F. 1999, P&SS, 47, 1305
Cravens, T. E., & Strobel, D. F. 2015, Icar, 246, 303
Dalle Ore, C., Morea Barucci, M. A., Emery, J. P., et al. 2009, A&A, 501, 349
Danger, G., Orthous-Daunay, F. R., de Marcellus, P., et al. 2013, GeCoA, 118, 184
Dangi, B. B., Kim, Y. S., Krasnokutski, S. A., Kaiser, R. I., & Bauschlicher, C. W. Jr. 2015, ApJ, 805, 76
Dangi, B. B., Maity, S., Kaiser, R. I., & Mebel, A. M. 2013, JPCA, 117, 11783
Dangi, B. B., Parker, D. S. N., Yang, T., Kaiser, R. I., & Mebel, A. M. 2014, Angewandte Chemie Int. Ed., 53, 4608
Dartois, E., Caro, G. M. M., Deboffle, D., Montagnac, G., & d'Hendecourt, L. 2005, A&A, 432, 895
de Marcellus, P., Meinert, C., Myrgorodska, I., et al. 2015, PNAS, 112, 965
DiSanti, M. A., & Mumma, M. J. 2008, SSRv, 138, 127
Drouin, D., Couture, A. R., Joly, D., et al. 2007, Scanning, 29, 92
Duvernay, F., Rimola, A., Theule, P., et al. 2014, PCCP, 16, 24200
Fang, M., Ivanisevic, J., Benton, H. P., et al. 2015, AnaCh, 87, 10935
Förstel, M., Maksyutenko, P., Jones, B. M., et al. 2015, Chem. Phys. Chem., 16, 3139
Förstel, M., Maksyutenko, P., Jones, B. M., et al. 2016, ChCom, 52, 741
Fraser, H. J., Collings, M. P., & McCoustra, M. R. S. 2002, RScI, 73, 2161
Gerakines, P., Schutte, W., & Ehrenfreund, P. 1996, A&A, 312, 289
Gillett, F., & Forrest, W. 1974, ApJL, 187, L37
Gladstone, G. R., Pryor, W. R., & Stern, S. A. 2015, Icar, 246, 279
Goulay, F., Osborn, D. L., Taatjes, C. A., et al. 2007, PCCP, 9, 4291
Griffith, C. A., Penteado, P., Rannou, P., et al. 2006, Sci, 313, 1620
Groner, P., Stolkin, I., & Gunthard, H. H. 1973, JPhE, 6, 122
Hammel, H. B., Lynch, D. K., Russell, R. W., et al. 2006, ApJ, 644, 1326
Hepp, M., & Herman, M. 1999, JMoSp, 197, 56
Herman, M. H. M. 1998, MolPh, 94, 829
Holler, B. J., Young, L. A., Grundy, W. M., Olkin, C. B., & Cook, J. C. 2014, Icar, 243, 104
Hudson, R., Gerakines, P., & Moore, M. 2014, Icar, 243, 148
Hudson, R. L., Moore, M. H., & Raines, L. L. 2009, Icar, 203, 677
Hunten, D. M. 2006, Natur, 443, 669
Ioppolo, S., Cuppen, H. M., Van Dishoeck, E. F., & Linnartz, H. 2011, MNRAS, 410, 1089
Irle, S., & Morokuma, K. 2000, JChPh, 113, 6139
Jackson, W. M., Faris, J., & Buccos, N. J. 1966, JChPh, 45, 4145
Jacox, M. E. 1962, JChPh, 36, 140
Jiménez-Escobar, A., & Caro, G. M. 2011, A&A, 536, 11
Jones, B. M., & Kaiser, R. I. 2013, JPhChL, 4, 1965
Jones, B. M., Zhang, F., Kaiser, R. I., et al. 2011, PNAS, 108, 452
Kaiser, R. I., Eich, G., Gabrysch, A., & Roessler, K. 1997a, ApJ, 484, 487
Kaiser, R. I., Gabrysch, A., & Roessler, K. 1995a, RScI, 66, 3058
Kaiser, R. I., Jansen, P., Petersen, K., & Roessler, K. 1995b, RScI, 66, 5226
Kaiser, R. I., Mahfouz, R. M., & Roessler, K. 1992, NIMPB, 65, 468
Kaiser, R. I., Maity, S., & Jones, B. M. 2014, PCCP, 16, 3399
Kaiser, R. I., Maity, S., & Jones, B. M. 2015, Angewandte Chemie Int. Ed., 54, 195
Kaiser, R. I., & Maksyutenko, P. 2015a, CPL, 631-632, 59
Kaiser, R. I., & Maksyutenko, P. 2015b, JPCC, 119, 14653
Kaiser, R. I., Maksyutenko, P., Ennis, C., et al. 2010, FaDi, 147, 429
Kaiser, R. I., & Roessler, K. 1992, AnGp, 10, 222
Kaiser, R. I., & Roessler, K. 1997, ApJ, 475, 144
Kaiser, R. I., & Roessler, K. 1998, ApJ, 503, 959
Kaiser, R. I., Stranges, D., Bevsek, H. M., Lee, Y. T., & Suits, A. G. 1997b, JChPh, 106, 4945
Khare, B., Thompson, W., Murray, B., et al. 1989, Icar, 79, 350
Kim, S. J. 2003, EP&S, 55, 139
Kim, Y. S., Bennett, C. J., Li-Hsieh, C., Brien, K. O., & Kaiser, R. I. 2010, ApJ, 711, 744
Kondo, S., & Saëki, S. 1973, AcSpA, 29, 735
Lattanzi, F., di Lauro, C., & Vander Auwera, J. 2011, JMoSp, 267, 71
Lavvas, P. P., Coustenis, A., & Vardavas, I. M. 2008, P&SS, 56, 67
Levin, I. W., Pearce, R. A., & Harris, W. 1973, JChPh, 59, 3048
Lias, S. G. 1982, Ion Cyclotron Resonance Spectrometry II (Berlin, Heidelberg: Springer)
Lias, S. G., Bartmess, J. E., Liebman, J. F., et al. 2016, in Ion Energetics Data, in NIST Chemistry WebBook, NIST Standard Reference Database Number 69, ed. P. J. Linstrom & W. G. Mallard, (Gaithersburg MD: National Institute of Standards and Technology) http://webbook.nist.gov, (retrieved March 31)
Lorenzi, V., Pinilla-Alonso, N., Licandro, J., et al. 2016, A&A, 585, A131
Mahajan, T. B., Elsila, J. E., Deamer, D. W., & Zare, R. N. 2002, OLEB, 33, 17
Maity, S., Kaiser, R. I., & Jones, B. M. 2014a, ApJ, 789, 36
Maity, S., Kaiser, R. I., & Jones, B. M. 2014b, FaDi, 168, 485
Maity, S., Kaiser, R. I., & Jones, B. M. 2015, PCCP, 17, 3081
Maksyutenko, P., Muzangwa, L. G., Jones, B. M., & Kaiser, R. I. 2015, PCCP, 17, 7514
Marcelino, N., Cernicharo, J., Agúndez, M., et al. 2007, ApJL, 665, L127
Meinert, C., Filippi, J. J., de Marcellus, P., d'Hendecourt, L. L., & Meierhenrich, U. J. 2012, ChemPlusChem, 77, 186
Modica, P., De Marcellus, P., Baklouti, D., et al. 2012, in EAS Publications Ser. 58, ed. C. Stehle, C. Joblin, & L. d'Hendecourt (Paris: EDP Sciences), 5
Moore, M. H., Ferrante, R. F., & Nuth Iii, J. A. 1996, P&SS, 44, 927
Moore, M. H., & Hudson, R. L. 1998, Icar, 135, 518
Mousis, O., Lunine, J. I., Hayes, A. G., & Hofgartner, J. D. 2016, Icar, 270, 37
Mousis, O., & Schmitt, B. 2008, ApJL, 677, L67
Muller, S., Combes, F., Guélin, M., et al. 2014, A&A, 566, A112
Mumma, M. J., DiSanti, M. A., Russo, N. D., et al. 1996, Sci, 272, 1310
Murphy, W. F., Fernandez-Sanchez, J. M., & Raghavachari, K. 1991, JPhCh, 95, 1124
Nakamura, R., Sumikawa, S., Ishiguro, M., et al. 2000, PASJ, 52, 551
Niemann, H. B., Atreya, S. K., Bauer, S. J., et al. 2005, Natur, 438, 779
Nixon, C. A., Jennings, D. E., Flaud, J. M., et al. 2009, P&SS, 57, 1573
Nyquist, I. M., Mills, I. M., Person, W. B., & Crawford, B. 1957, JChPh, 26, 552
Pacansky, J., & Dupuis, M. 1982, JAChS, 104, 415
Parker, D. S. N., Dangi, B. B., Kaiser, R. I., et al. 2014, JPCA, 118, 12111
Parker, D. S. N., Kaiser, R. I., Kostko, O., & Ahmed, M. 2015, Chem. Phys. Chem., 16, 2091
Parker, D. S. N., Zhang, F., Kaiser, R. I., Kislov, V. V., & Mebel, A. M. 2011, Chemistry-An Asian Journal, 6, 3035
Parker, D. S. N., Zhang, F., Kim, Y. S., et al. 2012, PNAS, 109, 53
Pilling, S., Andrade, D. P. P., da Silveira, E. F., et al. 2012, MNRAS, 423, 2209
Rawlings, J. M. C., Williams, D. A., Viti, S., & Cecchi-Pestellini, C. 2013, MNRAS, 436, L59
Ridgway, S. 1974, ApJL, 187, L41
Scheer, M. D., McNesby, J., & Klein, R. 1962, JChPh, 36, 3504
Sittler, E. C., Jr, Ali, A., Cooper, J. F., et al. 2009, P&SS, 57, 1547
Socrates, G. 2004, Infrared and Raman Characteristic Group Frequencies: Tables and Charts (New York, NY: Wiley)
Stephens, K. M., & Bauer, S. H. 1994, AcSpA, 50, 741
Strazzulla, G., Baratta, G. A., Domingo, M., & Satorre, M. A. 2002, NIMPB, 191, 714
Toftmann, B., Rodrigo, K., Schou, J., & Pedrys, R. 2005, ApSS, 247, 211
Tsegaw, Y. A., Sander, W., & Kaiser, R. I. 2016, JPCA, 120, 1577
Turner, A. M., Abplanalp, M. J., Chen, S. Y., et al. 2015, PCCP, 17, 27281
Turner, A. M., Abplanalp, M. J., & Kaiser, R. I. 2016, ApJ, 819, 97
Vakhtin, A. B., Heard, D. E., Smith, I. W. M., & Leone, S. R. 2001, CPL, 344, 317
van Nes, G. J. H. 1978, PhD thesis, Univ. Groningen
Vastel, C., Ceccarelli, C., Lefloch, B., & Bachiller, R. 2014, ApJL, 795, L2
Vuitton, V., Yelle, R. V., Lavvas, P., & Klippenstein, S. J. 2012, ApJ, 744, 11
Wisnosky, M. G., Eggers, D. F., Fredrickson, L. R., & Decius, J. C. 1983, JChPh, 79, 3513
Woon, D. E., & Park, J.-Y. 2009, Icar, 202, 642
Yang, T., Parker, D. S. N., Dangi, B. B., Kaiser, R. I., & Mebel, A. M. 2015, PCCP, 17, 10510
Yu-Jong, W., Shiang-Jiun, C., Sian-Cong, C., & Tzu-Ping, H. 2014, ApJS, 212, 7
Zhang, F., Jones, B., Maksyutenko, P., et al. 2010, JAChS, 132, 2672
Zhang, F., Kaiser, R. I., Kislov, V. V., et al. 2011, JPhChL, 2, 1731
Zhang, F., Kim, S., & Kaiser, R. I. 2009, PCCP, 11, 4707
Zhou, L., Dahbia, T., Evelyne, R., et al. 2013, ApJ, 765, 80
Zhou, L., Kaiser, R. I., Gao, L. G., et al. 2008, ApJ, 686, 1493
Zhou, L., Zheng, W., Kaiser, R. I., et al. 2010, ApJ, 718, 1243